FINITE ELEMENT ANALYSIS OF BOLTED JOINT SUBJECTED TO IMPACT LOADING

by

Niyazi Tanlak

B.S., Mechanical Engineering, Yıldız Technical University, 2005

Submitted to the Institute for Graduate Studies in
Science and Engineering in partial fulfillment of
the requirements for the degree of
Master of Science

Graduate Program in Mechanical Engineering
Boğaziçi University

2008

FINITE ELEMENT ANALYSIS OF BOLTED JOINT
SUBJECTED TO IMPACT LOADING

APPROVED BY:

Assoc. Prof. Fazıl Önder Sönmez (Thesis Supervisor)	.....
Asst. Prof. Nuri Ersoy	.....
Asst. Prof. Sami And Kılıç	.....

DATE OF APPROVAL: 11.09.2008

ACKNOWLEDGEMENTS

I would like to express my deepest gratitude to Assoc. Prof. Fazıl Önder Sönmez, my advisor for helping, guiding and encouraging me to finish this dissertation. Without his numerous suggestions, inspiring ideas, patience, and support, this work would have never been completed.

I would also like to thank to the members of the evaluation committee, who have spared their valuable time for the assessment of this work.

I am very grateful to my friends, who gave me the motivation that helped me to finish this work. There are many names, and for the fear of leaving one out accidentally, I will not try.

Platform ArGe AŞ - TOFAŞ is gratefully acknowledged for supporting this research.

Last but definitely not the least I thank my family for their support and understanding.

ABSTRACT

FINITE ELEMENT ANALYSIS OF BOLTED JOINT SUBJECTED TO IMPACT LOADING

Mechanical components are commonly fastened together through bolts. Many times, they are subjected to impact loads in use. The behavior of the joints under these conditions should be known in a design process. The objective of this study is to develop finite element models of bolted joints under impact loading. First, a three dimensional finite element model for a bolted joint was developed in order to simulate its behavior under impact loading. With this full modeling, the aim was to simulate the physics of the impact event as accurately as possible without giving any concern on computational cost. In the design of mechanical structures containing numerous fastening elements, use of full models is not practicable, because the computational cost of the analysis dramatically increases with increased number of complex interacting parts. Instead, simplified models accounting for only dominating effects should be utilized such that analysis time can significantly be reduced without sacrificing from the accuracy. Accordingly, a number of simplified finite element bolt models were developed and then compared with the full model regarding the solution accuracy and computational cost for different loading cases to determine the most representative and cost effective simplified model.

ÖZET

ÇARPIŞMAYA MARUZ CIVATALI BAĞLANTILARIN SONLU ELEMANLAR ANALİZİ

Mekanik parçalar yaygın olarak cıvatalar kullanılarak bağlanırlar. Kullanım süreleri sırasında çoğu zaman ani çarpışma yüklerine maruz kalırlar. Tasarım prosesinde cıvatalı bağlantının bu yükler altındaki davranışını bilmek gereklidir. Bu çalışmanın amacı ani çarpma yükleri altında cıvatalı bağlantılar için sonlu elemanlar modelleri geliştirmektir. Tam modelleme yaklaşımının amacı olayın fiziğini hesaplama maliyetlerini göze almaksızın mümkün olduğu kadar doğru simule etmektir. Birçok bağlantı elemanı içeren mekanik bir yapını tasarım aşamasında tam sonlu elemanlar modelini kullanmak pratik değildir. Zira analizin hesaplama maliyeti dramatik olarak artmaktadır. Bunun yerine sadece cıvatanın temel etkilerini yerine getiren basitleştirilmiş modeller kullanılarak analiz yükü önemli miktarda düşürülebilmektedir. Buna bağlı olarak hesaplama yükünü azaltarak cıvatalı bağlantının davranışını tahmin edebilen basitleştirilmiş sonlu elemanlar cıvata modelleri geliştirilmiştir. Daha sonra, en efektif modeli bulmak amacıyla değişik yükleme koşullarında sonuç doğruluğu ve hesaplama zamanı gibi kriterler kullanılarak basitleştirilmiş modeller tam modelle karşılaştırılmıştır.

TABLE OF CONTENTS

LIST OF FIGURES

LIST OF TABLES

LIST OF SYMBOLS / ABBREVIATIONS

d	Mass density
d_c	User-defined decay coefficient
E	Young's modulus
g	Gravitational acceleration
I	Moment of inertia
L^e	Element length
S_e	End distance of bolted joint from the hole
m	First exponential constant
n	Second exponential constant
t	Time
v	Velocity of the impactor
W	Weight
z	Through the thickness direction
μ_k	Kinetic friction coefficient
μ_s	Static friction coefficient
γ_{eq}	Slip rate
δ_{st}	Static deflection
δ_{max}	Maximum deflection
$\overline{\varepsilon}^{pl}$	Equivalent plastic strain,
$\dot{\overline{\varepsilon}}^{pl}$	Inelastic strain rate

BC	Boundary Condition
C3D8R	Continuum three dimensional 8-noded reduced integration
FEA	Finite Element Analysis
IC	Initial Condition
RHS	Right hand side

1. INTRODUCTION

Bolts are one of the most commonly used fastening elements in construction and in the assembly of mechanical structures. Bolted joints are used as fastening elements in almost every engineering application, ranging from construction to automotive applications. The structures with bolted joints are usually subjected to not only various static loads but also impact loads. Because bolts provide localized connection, they lead to high stress concentration. Considering that under impact loading extremely high level of stress may develop at the notches. The region around a bolt is one of the most critical locations. Designing for safety requires accurate determination of stress and strain states around the bolts under impact loading.

A bolted joint by itself is a very complex part considering the contact between teeth of the bolt and the nut, pretension in the bolt shank, contact surfaces between the nut and the washer, bolt head and the washer, washers and the sheets, bolt shank and the holes of the washers and the sheets. Commercial finite element codes are capable of simulating almost all complex phenomena. However, some difficulties that a numerical analyst should face are to develop appropriate models capable of providing an accurate representation of the physics with the lowest possible computational cost. Choice of constitutive law, integration scheme at the constitutive level, number of integration points, step size, kinematical description, element type and discretization depends upon problem, geometry, type of loading, required accuracy, simplification of complex geometries and so on.

1.1. Literature Survey

The researchers were generally interested in bolted joints subjected to static loadings[1-14]. Mistakidis ve Baniotopoulos [1] used plane stress elements to model the bolted joints without considering the pretension in the bolt. A number of researches [2, 3, 4, 11], modeled bolts and nuts using three dimensional elements with and without pre-tensioning order for the model to be as realistic as possible. In some studies [3,4], bolts were modeled using beam elements. In one study [13], the nut and the head of the bolt

were modeled using brick elements and the bolt shank was modeled using beam elements. Kishi *et al.* [7] modeled the nut and the head of the bolt as hexagonal rather than cylindrical. Like the researchers [8, 10, 15, 16] who took the pretension of bolts into account, Swanson *et al*. [8] applied the clamping force via a prescribed displacement. Barth *et al*. [9] assumed the bolts to be rigid. Citipitioglu *et al*. [10] assumed the pre-tensioning in two steps: first, the length of the bolt was chosen to be shorter than the total thickness of the joined plates. In the second step, the contact between the displaced bolt head and its respective surface was activated and the imposed displacement was released. Some researchers [15, 16] frequently gave artificial coefficients of thermal expansion to the bolt shank to induce pretension. In another study [14], that coefficient was applied to one of the washers. Chung ve Ip [5,6] artificial small holes which do not affect the behavior of the joint were made through the centre-axis of the bolts for ease of meshing.

The bolted joints subjected to dynamic loadings were rarely studied in comparison with the static studies [15, 16, 17, 18, 19]. Sabuwala ve Linzell [17] analyzed the bolts joint subjected to blast and cyclic loads. The bolt and the nut were modeled as separate parts contrary to the models in which nuts were integral parts of the bolts. Reid ve Hiser [18] modeled the nut and the head of the bolt in hexagonal shape and included the washers into the analysis. They assumed the bolt either as rigid or deformable in various analyses. Oldfield *et al*. [19] induced the pretension of the bolt by using implicit solver, then imported the results to the explicit solver and analyzed the structure under cyclic loading via explicit solver in order to reduce the computational time. Kwon *et al*. [15] introduced both a three dimensional full bolt model and some simplified bolt models. In one of the simplified models, the bolt head and the nut were modeled with shell elements, whereas the shank of the bolt with solid elements. In another simplified model, the entire bolt-nut assembly was modeled with shell elements. Kim *et al*. [16] used various simplified bolt models to find natural frequency of the structure. Hendricks and Wekezer [20] merged the nodes between the separate parts in order to model the bolts. In an alternative simplified model tie constraints were used. O'Daniel *et al*. [21] used connecting beam elements through the mesh of the panels in order to adopt the bolted joints.

Detailed information is given in Appendix A.

So far, the researchers usually interested in bolted joints under static load, which did not reach high strain values on the sheets. There were some studies about the joints under impact loads. But they did not focus on around the bolt hole. Besides, the aim of the studies which were related to impact loads was mainly to predict the physics of the problem without regarding computational concerns.

2. PROBLEM STATEMENT

In automotive applications, usually thin panels are used that are joined by bolts or spot welds. For this reason, panels are expected to fail not bolts. Failure generally occurs where the impactor hits the panel or around the bolts. There are three modes for the failure at the perimeter of the bolt holes, which are bearing failure, shear-out failure and net-section failure. Bearing failure occurs when the distance between the hole of the bolt and the end of the plate as well as the distance between the hole and the closest side of the plate are sufficient to withstand to loads, as seen Figure 2.1.b. When the end distance, S_e, is small as compared with the bolt diameter, the shear-out failure takes place. The net-section failure occurs in bolted joints, accompanied by necking of the net-section, $\frac{S_c}{2} - R$, when the side distance of the plate to the bolt hole is not enough to withstand to the loads (see Figure 2.1). So the simplified models should predict the plastic strains on perimeter of the bolt holes due to the importance of that.

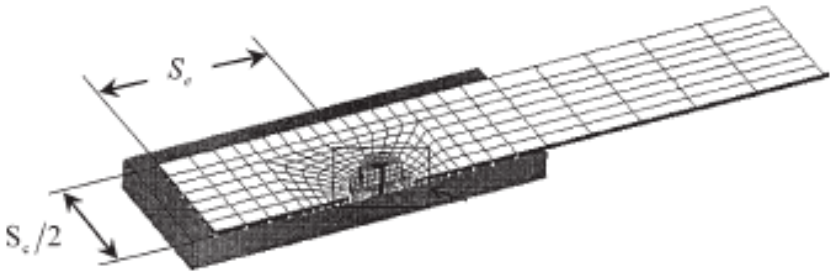

Figure 2.1. End distance of a bolted joint [5]

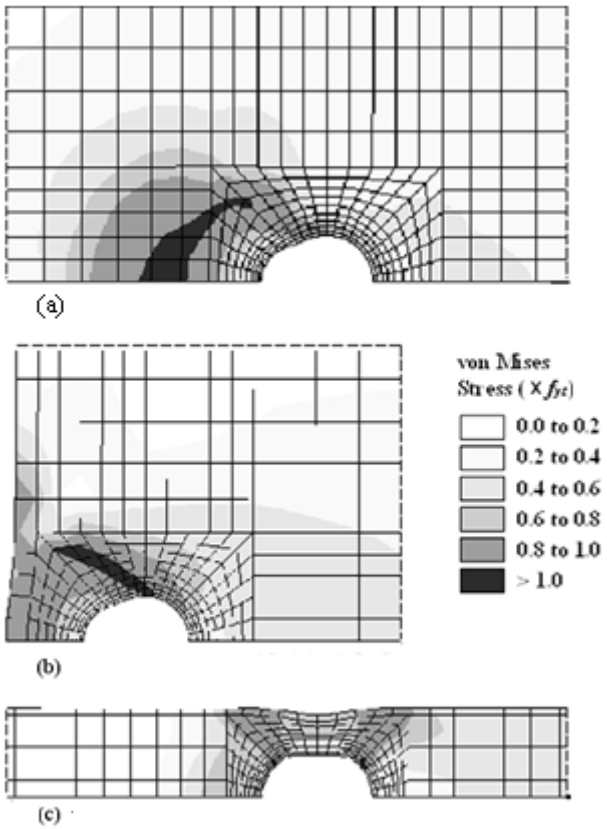

Figure 2.2. Failure modes of the panels of a bolted joint a) bearing failure b) shear-out failure c) net-section failure [5]

. A full model of a bolted joint accounting for all aspects of the physics of the problem requires taking into account many contact relations between different components of the joint. Considering that even a simple panel may contain many fasteners, analyzing the structure with all its complexity leads to excessively times. This makes the use of full model impractical in typical applications of engineering design. So there is a need for a finite element bolt model that reduces the complexity of the geometry and the number of contact relations so that analysis can be completed in a relatively short time without much compromising from the accuracy .

In this study, the bolted joint subjects to high plastic strain values under high strain rates. The strain values around the bolt holes are interested.

3. METHODOLOGY

Under impact loadings, the structures are usually analyzed via explicit finite element codes because of the transient nature of the phenomenon. Explicit methods require a small time increment size that depends solely on the highest natural frequencies of the model and is independent of the type and duration of loading. Simulations generally take on the order of 10,000 to 1,000,000 increments, but the computational cost per increment is relatively small. Implicit methods do not place an inherent limitation on the time increment size; increment size is generally determined from accuracy and convergence considerations. Implicit simulations typically take orders of magnitude fewer increments than explicit simulations. However, since a global set of equations must be solved in each increment, the cost per increment of an implicit method is far greater than that of an explicit method. The explicit dynamics method was originally developed to analyze high-speed dynamic events that can be extremely costly to analyze using implicit programs. Since the load is applied rapidly and is very severe, the response of the structure changes rapidly. Accurate tracking of stress waves through the plate is important for capturing the dynamic response. Since stress waves are associated with the highest frequencies of the system, obtaining an accurate solution requires many small time increments. Furthermore, contact conditions are formulated more easily using an explicit dynamics method than using an implicit method. Explicit methods can readily analyze problems involving complex contact interaction between many independent bodies. Explicit methods is particularly well-suited for analyzing the transient dynamic response of structures that are subject to impact loads and subsequently undergo complex contact interaction within the structure [23] For all these reasons, ABAQUS/Explicit is used in this study.

But first of all, there should be at least two structure configurations used for numerical in order to confirm the repeatability of the numerical studies for working properly in various conditions. In the numerical study, there is a need for a finite element bolt model that reflects all aspects of the physics of the problem. That model should be in a three dimensional manner and be modeled using three dimensional elements. That model is called as full bolt model in this study. Full bolt model neglects the teeth of the bolts. It

considers the nut as an integral part to the bolt. The nut and the bolt head is considered as cylindrical not hexagonal. The chamfers and the fillets of the bolt are neglected either. The washers of the bolt are included into the full model. They are considered as deformable like the rest of the bolt-nut assembly. That model is used for further comparisons during the development of new simplified models. Namely, the full bolt model is a benchmark for simplified models in terms of computational cost and computer memory capacity needed and accuracy in numerical part of this study. There is a need to the simplified models developed for the bolted joints, which they makes the solution of the problem easier, and decreases the computational time, simulates the overall physics of the so-called problem in a acceptable way.

Simplified models neglects what the full model neglects. Their main aim is to mimic the behavior of the bolt. Namely, that is to hold the plates together and to transmit the forces between the plates. By considering those purposes, the simplified models usually were developed in a way that they need only one contact relations apart from the impact zone, which is between the sheets of the joint. The only exception to this rule is the simplified Model 11 which has four contact relations.

4. DETAILED FINITE ELEMENT MODELING OF BOLTED JOINTS: FULL MODEL

ABAQUS version 6.5 is used in the all analyses. The Abaqus product suite comprises of three core products: Abaqus/Standard, Abaqus/Explicit and Abaqus/CAE. Abaqus/Standard is a general-purpose solver using a traditional implicit integration scheme to solve engineering problems. Abaqus/Explicit uses explicit integration scheme to solve highly nonlinear transient dynamic and quasi-static problems. Abaqus/CAE provides an integrated modeling (preprocessing) and visualization (postprocessing) environment for the analysis inputs and results, respectively [22].

In this model, obtaining accurate results regardless of the computational burden was aimed. For this reason, the bolt model was made as detailed as possible. Nevertheless, some features of the geometry that are assumed to have insignificant effect on the response of the joint were ignored. Firstly, the threads of the bolt and the nut were ignored. The bolt-nut assembly was modeled as monolithic. In other words, the nut was an integrated part of the bolt considering that relative motion between bolt and nut, or loosening will not take place during impact. This assumption is justified. Secondly, the bolt head and the nut were modeled as cylindrical rather than hexagonal considering that pressure is applied by the washers and meshing of hexagonal shapes is difficult. The other features of the geometry were accounted for in the model. The washers were modeled separately. All of the components were taken as deformable.

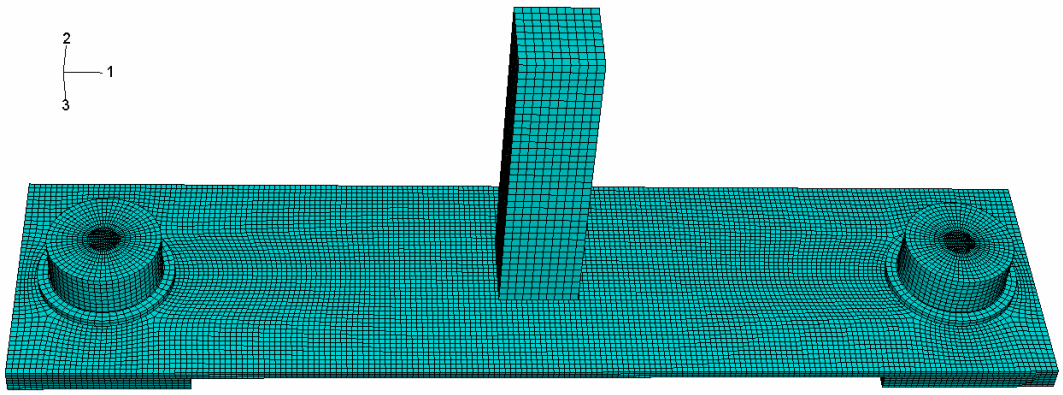

Figure 4.1. The model for the whole set-up

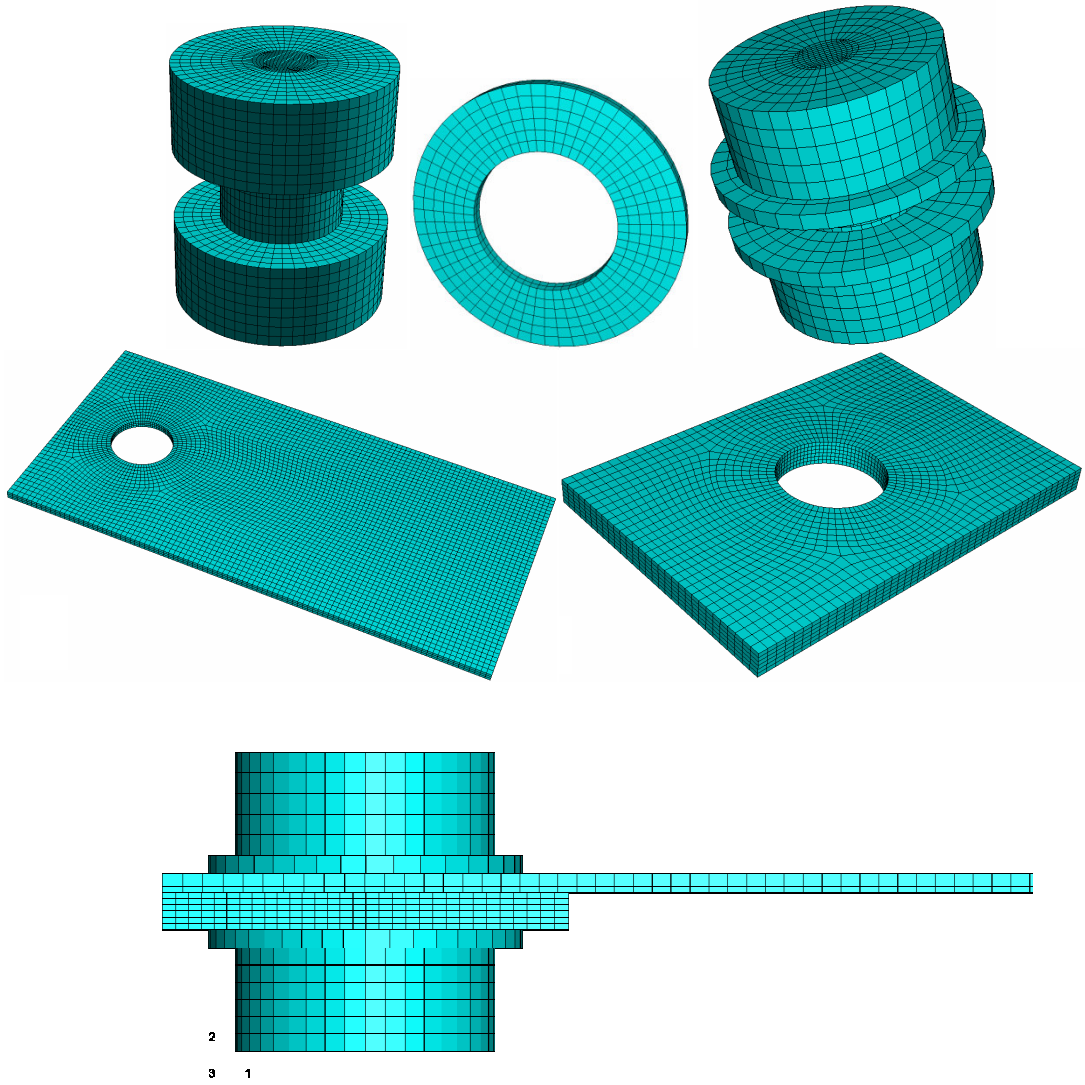

Figure 4.2. The geometry of the components in the full model for one of the symmetric parts

4.1. Model Geometry of the Joined Sheets

In this study, the experimental set-up depicted in Figure 4.1 is simulated. A sheet of material called “plate” is fastened by a single bolt at each end to a thicker sheet called “frame”, which is in turn fixed to the main frame. The plate is hit at the middle by an impactor dropped at a certain height. Benefiting the symmetry of the structure, half of it is analyzed. Figure 4.2 showed the geometries and the finite element mesh of the individual components in the joint. The plate has a thickness of 1 mm, while the frame has a thickness of 2 mm. The hole has a radius of 4.2 mm. The other dimensions are given in Figure 4.3.

Two different geometric configurations were used. The only difference between the two configurations is the length of the frame, which is 24 mm in configuration 1, 22 mm in configuration 2. The bolt has typical dimensions of M8 bolt. Namely, its shank has a radius of 4 mm, its bolt head has a width of 14 mm across its corners, and a thickness of 5.6 mm.

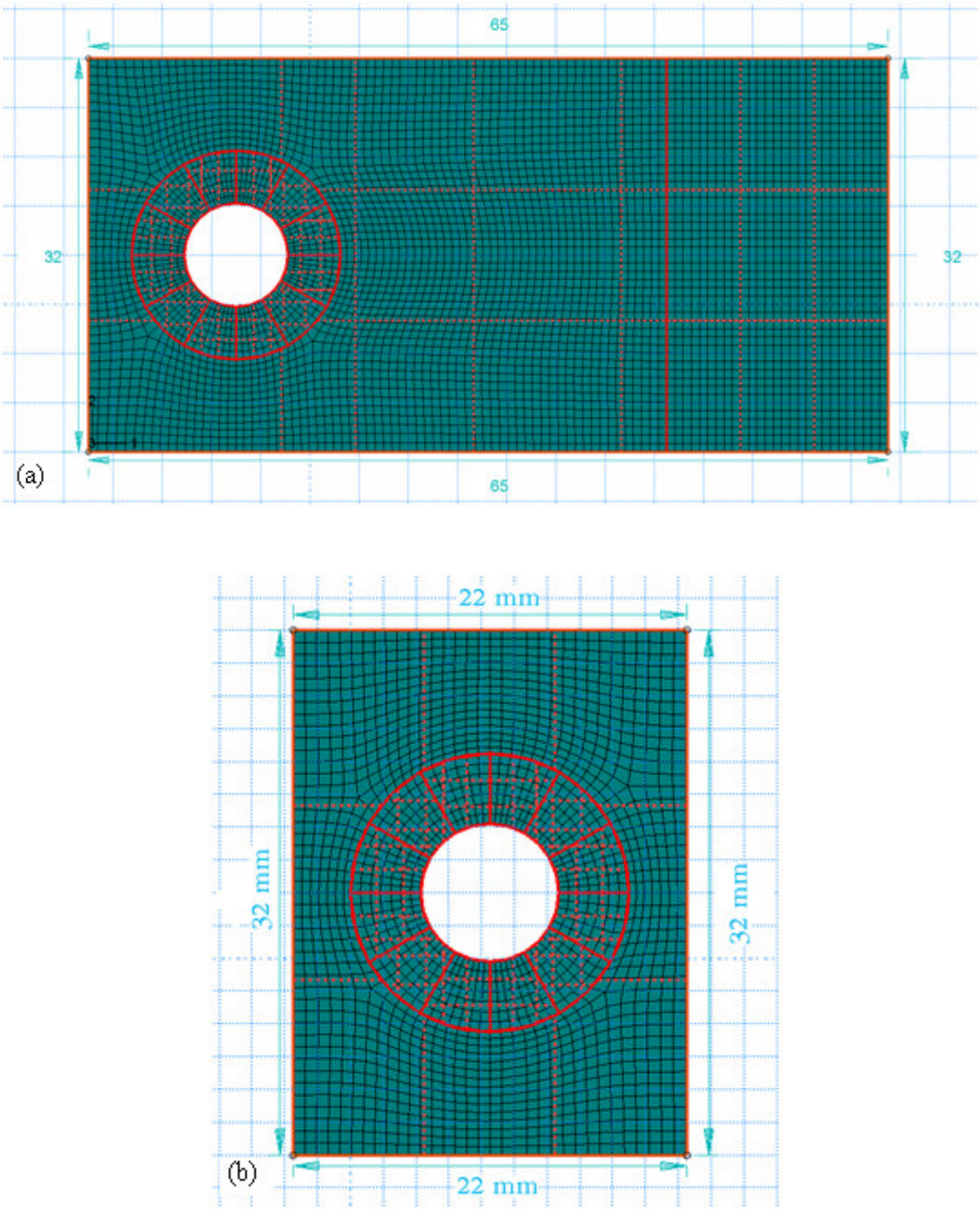

Figure 4.3. Dimensions of the plate (a) and the frame (b) for configuration 2

The washers have a thickness of 1 mm. Its inner and outer radii are given in Figure 4.?.

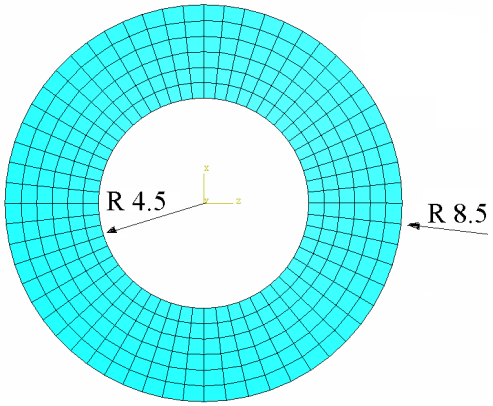

Figure 4.4. Dimensions of the washer

4.2. Material model

Generally, a material's yield stress, $\bar{\sigma}$ is dependent on work hardening, which for isotropic hardening models is usually represented by a suitable measure of equivalent plastic strain, $\bar{\varepsilon}^{pl}$; and inelastic strain rate, $\dot{\bar{\varepsilon}}^{pl}$:

$$\bar{\sigma} = \bar{\sigma}\,(\bar{\varepsilon}^{pl}, \dot{\bar{\varepsilon}}^{pl}) \tag{4.1}$$

Mechanical behavior of materials under impact loading depends on strain rate. As strain rates increase, many materials show an increase in their yield strength. The material of sheets joined by bolts was chosen to be steel. Experimentally determined strain-rate dependent stress-strain relations were used in the simulation. The data were provided for strain rates between 0.00 m/m.sec, namely under quasi-static condition, and 500.00 m/m.sec as shown in Figure 4.5. Besides, the material has an elastic modulus 205 GPa, Poisson's ratio of 0.33 and a density of 7800$\frac{kg}{m^3}$.

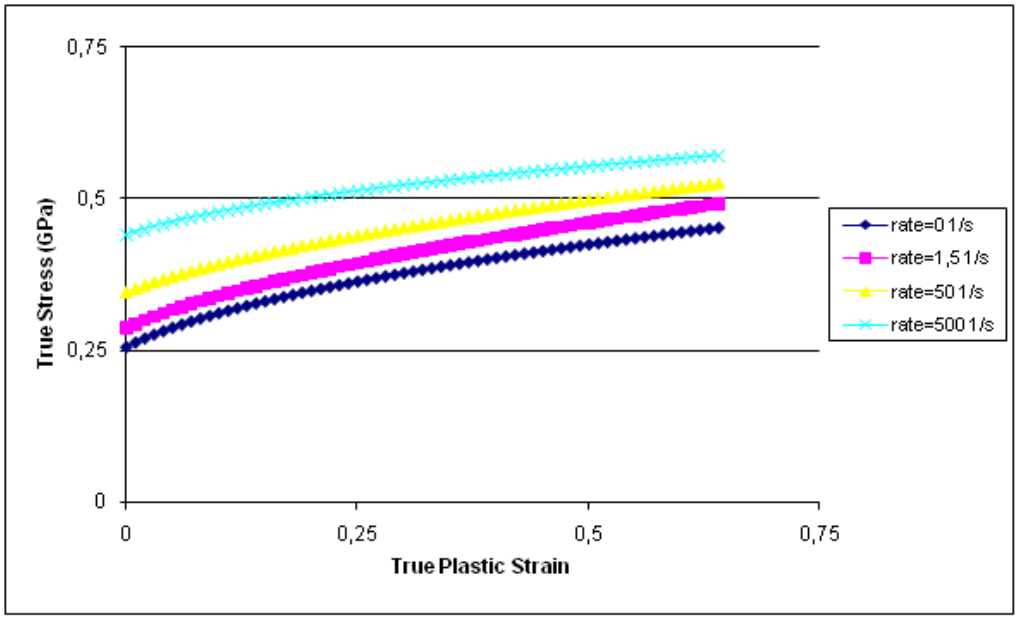

Figure 4.5. True stress-strain curve of the material under different strain rates in the plastic region

Projectile material properties are as follows; Young's modulus of 400 GPa, Poisson's ratio of 0.3, and density of 3000 kg/m^3. Besides, the bolt material has the properties of 210 GPa of Young's modulus, Poisson's ratio of 0.3, yield strength of 240 MPa.

4.3. Meshing

Selection of an appropriate type of element for the finite element model is crucial in order to obtain reliable results. A set of requirements should be satisfied by the selected elements type: Firstly, the element should have large strain and large deflection capabilities in order to account for large deformations experienced by the structure during impact. Secondly, because the full model should be based on 3D geometry of the bolted joint, the element types have to be compatible with it. Thirdly, we have to choose element integration type out of two options which are full and reduced integrations. The expression of "full integration" refers to the number of Gauss points required to exactly integrate the polynomial terms in an element's stiffness matrix with a regular shaped element. For hexahedral and quadrilateral elements a "regular shape" means that the edges are straight and meet at right angles and that any edge nodes are at the midpoint of the edge. Fully

integrated, linear elements use two integration points in each direction. Thus, the three-dimensional element C3D8 uses a 2 × 2 × 2 array of integration points in the element.

There is a problem in linear elements with full integration. Namely, it is shear locking. Shear locking causes the elements to be too stiff in bending. It is explained as follows. Consider a small piece of material in a structure subject to pure bending. The material will distort as shown in Figure 4.6. Lines initially parallel to the horizontal axis take on constant curvature, and lines through the thickness remain straight. The angle between the horizontal and vertical lines remains at 90°.

Figure 4.6. Deformation of material subjected to bending moment M

The edges of a linear element are unable to curve; therefore, if the small piece of material is modeled using a single element, its deformed shape is like that shown in Figure 4.7.

Figure 4.7. Deformation of a fully integrated, linear element subjected to bending moment M

Dotted lines that pass through the integration points are plotted for visualization purposes. It is obvious that the upper line has increased in length, indicating that the direct stress in the 1-direction, σ_{11}, is tensile. The length of the lower dotted line has decreased, indicating that σ_{11} is compressive. The length of the vertical dotted lines has not changed (assuming that displacements are small); therefore, σ_{22} at all integration points is zero. All this is consistent with the expected state of stress of a small piece of material subjected to pure bending. But the angle between the vertical and horizontal lines at each integration point, which was initially 90°, has changed. This shows that the shear stress, σ_{12}, at these points is nonzero. Actually this is not correct: the shear stress in a piece of material under pure bending should be zero [23].

This artificial shear stress arises due to inability of the edges of the element to curve. Its existence means that some of the strain energy is creating shearing deformation rather than the intended bending deformation, so the overall deflections are smaller and then the element is too stiff.

Shear locking solely affects the performance of fully integrated linear elements subjected to bending loads. These elements function perfectly well under direct or shear loads. Shear locking is not an issue for quadratic elements since their edges are able to curve.

Fully integrated linear elements should be used only when it is fairly certain that the loads will produce minimal bending in your model. Using a different element type will be more appropriate if there are doubts about the type of deformation the loading will create. Fully integrated quadratic elements can also lock under complex states of stress; thus, the results should be checked carefully if they are used exclusively in the model. However, they are very useful for modeling areas where there are local stress concentrations.

On the other hand, reduced-integration elements use one fewer integration point in each direction than the fully integrated elements. Reduced-integration linear elements have just a single integration point located at the element's centroid [23].

Linear reduced-integration elements tend to be too flexible because they suffer from their own numerical problem called hour-glassing. Again, consider a single reduced-integration element modeling for a small piece of material subjected to pure bending (see Figure 4.8).

Figure 4.8. Deformation of a linear element with reduced integration subjected to bending moment M

The length of the dotted lines, as well as the angle between them does not change, which means that all components of strain at the element's single integration point are zero. This bending mode of deformation is thus a zero-energy mode because no strain energy is

generated by this element distortion. The element is unable to resist this type of deformation since it has no stiffness in this mode. In coarse meshes this zero-energy mode can propagate through the mesh, producing meaningless results.

In ABAQUS a small amount of artificial “hourglass stiffness” is introduced in first-order reduced-integration elements to limit the propagation of hourglass modes. This stiffness is more effective at limiting the hourglass modes when more elements are used in the model, which means that linear reduced-integration elements can give acceptable results as long as a reasonably fine mesh is used. The errors arising with the finer meshes of linear reduced-integration elements are within an acceptable range for many applications. The results suggest that at least four elements should be used through the thickness when modeling any structures carrying bending loads with this type of element. When a single reduced-integration linear element is used through the thickness of a beam or plate, all the integration points lie on the neutral axis and the model is unable to resist bending loads [23].

By taking all these considerations into account regarding element, three dimensional continuum hexahedron 8-node linear brick elements (C3D8R) with reduced integration and hourglass control, were used to generate finite element mesh on the solid models of the frame, the plate, bolt-nut, and the washers as shown in Figure 4.2. The integration point of the C3D8R element is located at the middle of the element. The advantage of using the reduced integration elements is that the strains and stresses are calculated at the locations that provide optimal accuracy. A second advantage is that the reduced number of integration points decreases storage requirements and CPU time. The disadvantage is that the reduced integration procedure can admit deformation modes that cause no straining at the integration points. These zero-energy modes make the element rank-deficient and cause a phenomenon called “hour-glassing,” where the zero energy mode starts propagating through the mesh, leading to inaccurate solutions. This problem is particularly severe in first-order quadrilaterals and hexahedra. To prevent these excessive deformations, an additional artificial stiffness is added to the element. In this so-called hourglass control procedure, a small artificial stiffness is associated with the zero-energy deformation modes [23].

No wedge elements were used in the model. The frame and the plate were also modeled using brick elements. Contacting surfaces had similar meshes.

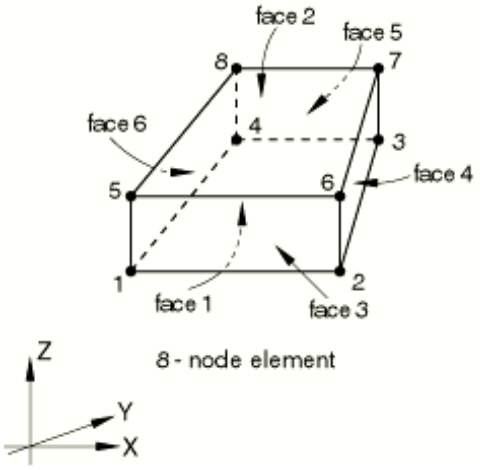

Figure 4.9. Geometry, node location and the coordinate system for C3D8R

Figure 4.10 shows a typical mesh density for a model of the frame, bolt, washer, and a symmetric part of the plate and the impactor.

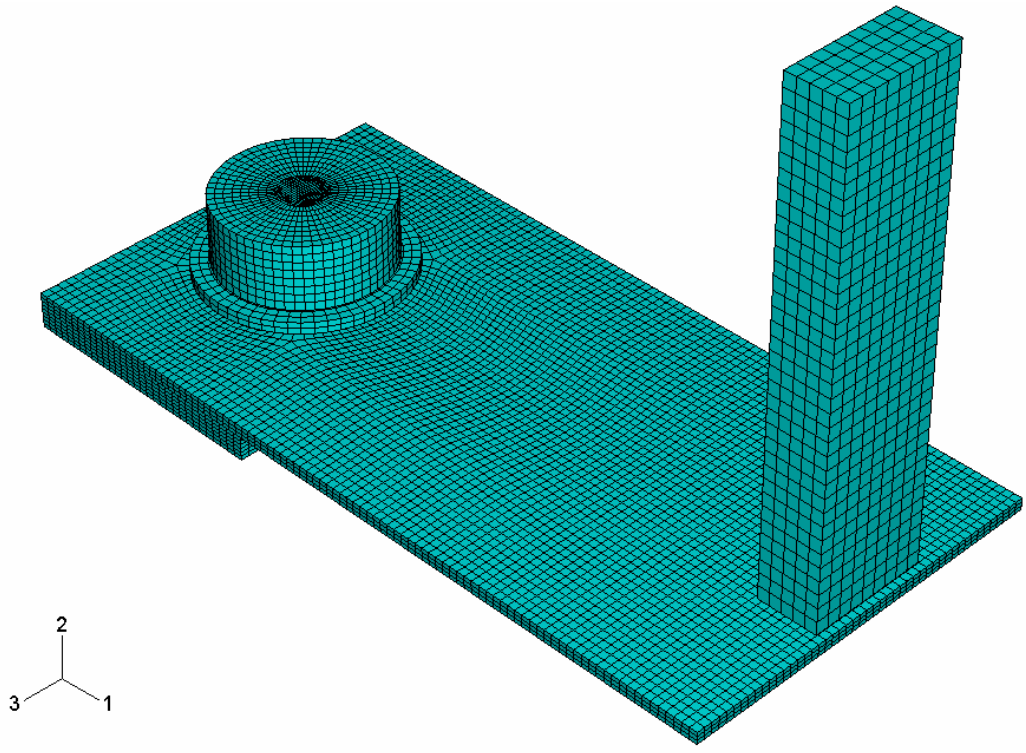

Figure 4.10. Typical mesh pattern of the full model

4.4. Boundary Conditions

An appropriate choice of the boundary conditions is vital to achieve a realistic simulation. The un-deformed mesh and boundary conditions are shown in Figure 4.6. Half of the plate is modeled to save computational time benefiting from its symmetry. Fully fixed boundary conditions are specified on one side of the frame and symmetry conditions are specified on the plate at the cutting plane. The impactor has a length of 40 mm and a rectangular cross section of 10x10 mm. Half of it is modeled with symmetry conditions specified on the cutting plane. The joint and the impactor are subjected to a gravitational field of 9.81 in the negative direction of 2-axis. The plates are hit by various impactors with different velocities and masses. In configuration 1, the density and the velocity of the impactor are 20000 kg/m^3 and 5 m/2, respectively. In configuration 2, these are 30000 kg/m^3 and 25 m/s.

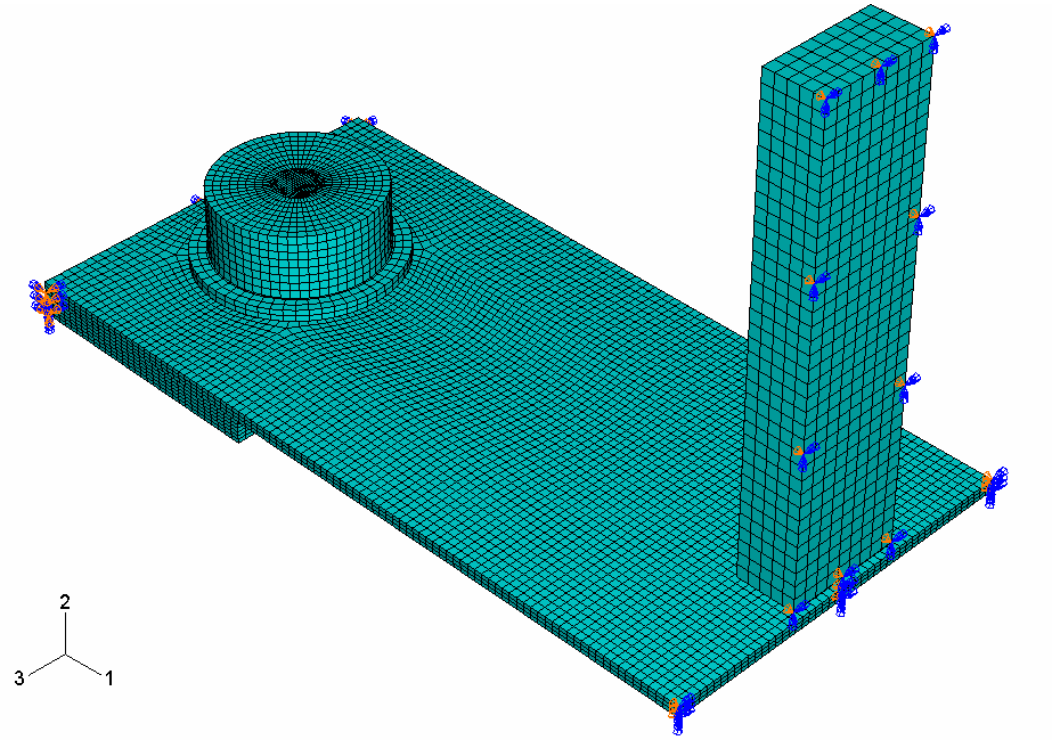

Figure 4.11. Boundary conditions

4.5. Contact

One of the key issues in the analysis of bolted joints is how to simulate interacting components. In this study, the contact between the plate and the impactor is modeled by finite-sliding contact with penalty contact enforcement. There are some reasons to opt for the penalty contact enforcement over kinematic contact enforcement on the location where the impact occurs. Firstly, the method of kinematic contact enforcement brings about kinetic energy losses in contacting nodes. This energy loss can be significant with a coarse mesh. Secondly, the penalty contact algorithm can model some types of contact that the kinematic contact algorithm cannot. Therefore, the penalty contact enforcement method is employed to enforce the contact compatibility between contacting surfaces.

Contacting surfaces in the joint have almost identical meshes. This helps to improve the analysis time.

Ten contact pairs are created in the full finite element model as follows:

Contact pair 1: The bottom surface of the impactor and a part of the top surface of the plate.

Contact pair 2: The bottom surface of the plate and the top surface of the frame.

Contact pair 3: The bottom surface of the head of the bolt and the top surface of the corresponding washer.

Contact pair 4: The top surface of the plate and the bottom surface of the corresponding washer.

Contact pair 5: The bottom surface of the frame and the top surface of the corresponding washer.

Contact pair 6: The top surface of the nut and the bottom surface of the corresponding washer.

Contact pair 7-8: The surface of the bolt shank and the inner surfaces of the washers

Contact pair 9: The surface of the bolt shank and the inner surface of the bolt hole on the plate..

Contact pair 10: The surface of the bolt shank and the inner surface of the bolt hole on the frame.

4.6. Friction Model

When surfaces are in contact they usually transmit shear as well as normal forces across their interface. There is generally a relationship between these two force components. The relationship is usually expressed in terms of the stresses at the interface [23].

The static friction coefficient corresponds to the value given at zero slip rate and the kinetic friction coefficient corresponds to the value given at the highest slip rate. The transition between static and kinetic friction is defined by the values given at intermediate slip rates.

ABAQUS also provides a model to specify a static and a kinetic friction coefficient directly. In this model it is assumed that the friction coefficient decays exponentially, as can be seen in Figure 4.12, from the static value to the kinetic value according to the formula of $\mu = \mu_k + (\mu_s - \mu_k)e^{-d_c\gamma_{eq}}$ where μ_k is the kinetic friction coefficient, μ_s is the static friction coefficient, d_c is a user-defined decay coefficient, and γ_{eq} is the slip rate. This model can be used only with isotropic friction and does not allow dependence on contact pressure, temperature, or field variables. In this study, the static friction coefficient is 0.15; the kinetic friction coefficient is 0.12; decay coefficient is 1.

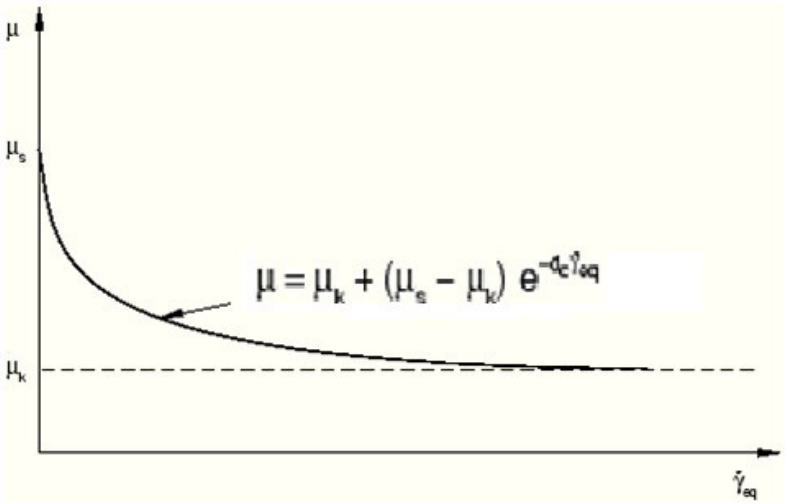

Figure 4.12. Exponential decay friction model [23]

4.7. Time Increments

The time increment used in an analysis must be smaller than the stability limit of the central-difference operator. Failure to use a small enough time increment will result in an unstable solution. If the solution becomes unstable, the time history response of solution variables such as displacements will usually oscillate with increasing amplitudes. The total energy balance will also change significantly. If the model is composed of only one material type, the initial time increment is directly proportionate to the size of the smallest element in the mesh. When the mesh contains uniform size elements but contains multiple material descriptions, the element with the highest wave speed will determine the initial time increment.

In nonlinear problems, those with large deformations and/or nonlinear material response, the highest frequency of the model will continually alter, which consequently changes the stability limit. Abaqus/Explicit uses two strategies for time incrementation control: fixed time incrementation and fully automatic time incrementation (where the code accounts for changes in the stability limit). Since Abaqus/Explicit will not check whether the computed response is stable or not during the step when fixed time incrementation is used. The user should ensure that a valid response has been obtained by carefully checking the energy history and other response variable [23]. Because of the difficulty of finding proper time in the fixed incrementation, in this study, the automatic one was employed.

In an analysis, Abaqus/Explicit initially uses a stability limit based on the highest element frequency in the whole model. Using the current dilatational wave speed in each element, this element-by-element estimate is determined:

$$\Delta t_{stable} = \frac{L^e}{\sqrt{\frac{E}{d}}} \tag{4.2}$$

where L^e is element length, d is mass density, E is Young's modulus (In this calculation, the stable time increment should be 1.29E-6, which corresponds to 0.66 mm mesh size.). The element-by-element estimate is conservative; it will give a smaller stable time increment than the true stability limit that is based upon the maximum frequency of the

entire model. In general, constraints such as boundary conditions and kinematic contact have the effect of compressing the eigenvalue spectrum, and the element-by-element estimates do not take this factor into account [23].

To compare the results of different models of bolted joints, one needs a stability limit estimation method that is applicable to all types of analyses. In some of the simplified models, thick beams are used (thickness to length ratio larger than 1.0), which do not permit the use of the global estimation algorithm. For this reason, the element-by-element stability estimation was opted over the global estimator.

5. SIMPLIFIED FINITE ELEMENT MODELS

All simplified models were compared with the full model in terms of accuracy, computational time and memory capacity needed. In order to reach a meaningful comparison, all parameters including mesh pattern contact enforcement methods and so on were chosen to be the same in all models.

A number of models were proposed to simulate the clamping effect of bolted joints in a simplifying manner by accounting for only dominating factors. Then, they were compared in terms of accuracy and computational time. In the simplified models shell elements were used to model the metal sheets considering that the thickness is very small in comparison to the lateral lengths. The element type used in the models is S4R, a 4-node, quadrilateral, shell element with reduced integration and a large-strain formulation, as shown in Figure 5.1. Simpson thickness integration rule is applied using five thickness integration points.

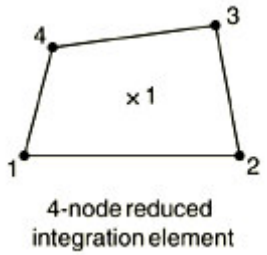

Figure 5.1. 4-node reduced integration shell element [23]

5.1. Simplified Model 1: Full Model with Shell Plates

In this model, the model for the bolt-nut assembly is the same as the full model; but the plate and the frame are discretized using shell elements considering that their thickness-to-lateral length ratio is less than 1/10. Actually, in all of the simplified models, sheets are modeled with shell element. The shells are positioned at the mid-surface of the sheets as seen in Figure 5.2. The same contact pairs as in the full model are defined in this model. A typical mesh pattern of this model can be seen in the Figure 5.3.

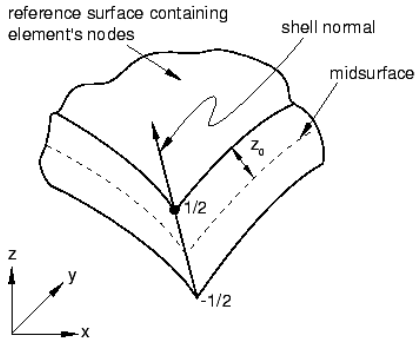

Figure 5.2. Mid-surface of a plate [23]

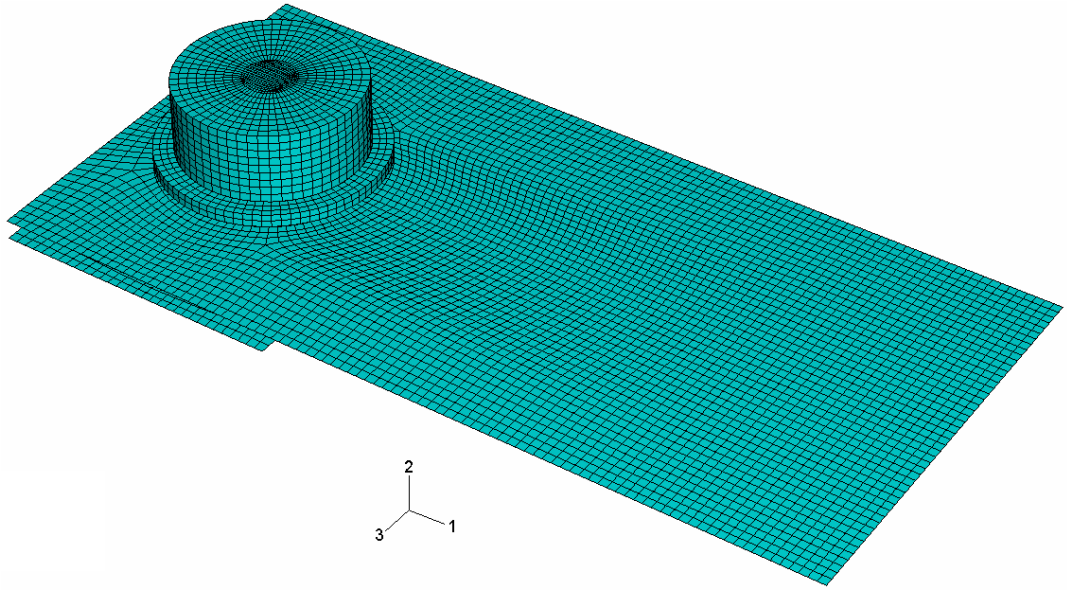

Figure 5.3. Simplified model 1

5.2. Simplified Model 2: Rigid shank and Coupling Constraints

In this model, the shaft of the bolt is modeled with solid elements (see Figure 5.4). Its material, however, is chosen as rigid considering that it is much stiffer than the sheet because of its large diameter in comparison to the thickness of the sheet. The effects of the bolt head and nut are simulated through coupling constraints. The central nodes on the upper and the lower surfaces of the cylinder are used as control points for the coupling constraints. The constraints are applied to the surfaces of the sheets that are under direct clamping pressure of the washers. The distributing coupling constraint is used in which all degrees of freedom are restrained. In this way, the relative motion between the ends of the bolt shank and the compressed region on the sheets is prevented. This means that the bolt

head, nut, and washers are also assumed to be non-deformable. The contact pairs 1, 2, 9, and 10 are introduced in this model.

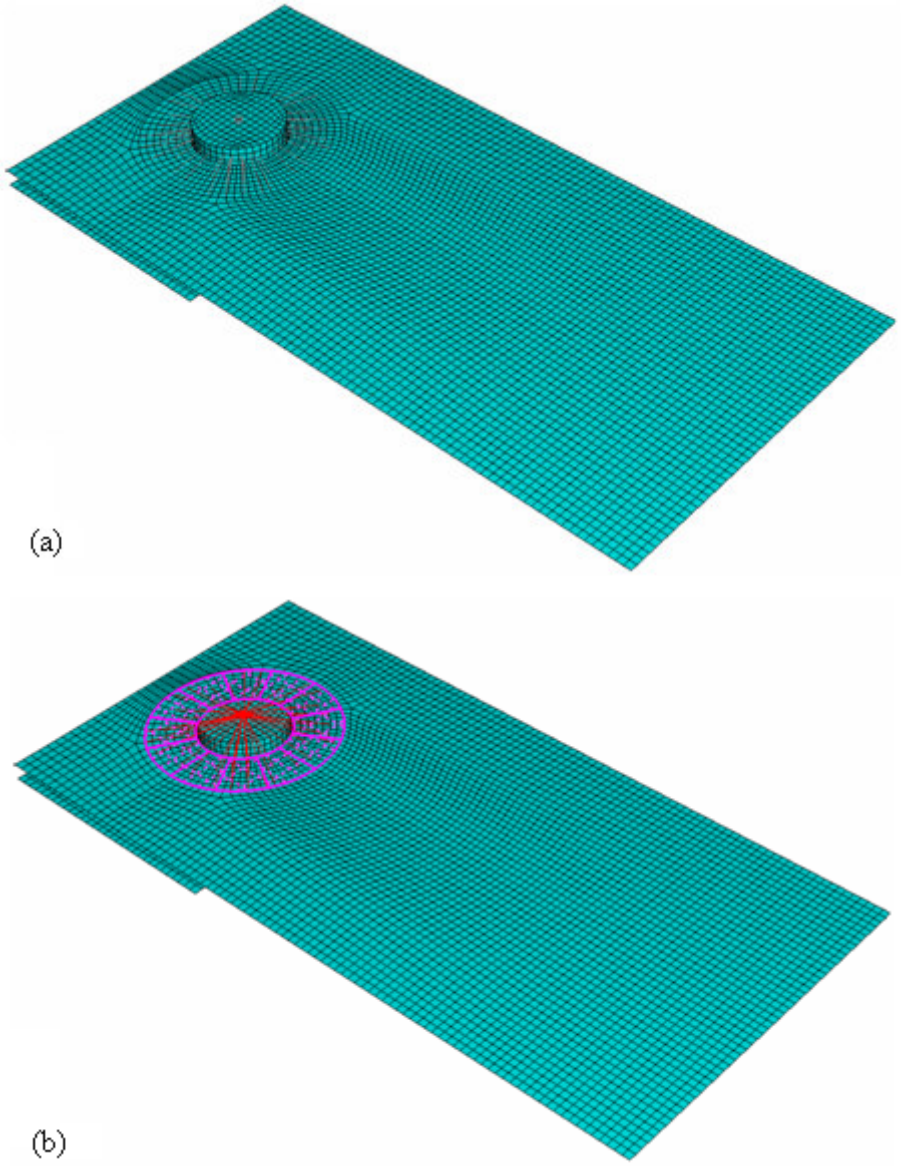

Figure 5.4. Simplified model 2 a) an overall view of the model b) a marked view of coupling constraints on the model

5.3. Simplified Model 3: Timeshenko Beam-Coupling Constraint

In this simplified model, the bolt shaft is modeled using a Timoshenko beam, B32, a 3-node quadratic beam element. This type of beam element accounts for the effects of the shear stress, which makes it suitable for short beams like bolt shank. The two nodes at the tips of the beam are chosen as the control points for the coupling constraints that restrain

the relative motion between the end of the beam and the region of the plate or frame which is in contact with the washer as shown in Figure 5.5. These constraints simulate the effects of the clamping pressure of bolt head and nut. In this model, only contact pairs 1 and 2 which are between the frame and the plate, and between the plate and the impactor are introduced; no contact relation is considered between the bolt shank and the holes. This model resembles to the model proposed by Kim *et al.* [16] but the sheets are discretized using shell elements in this model while they were discretized using brick element.

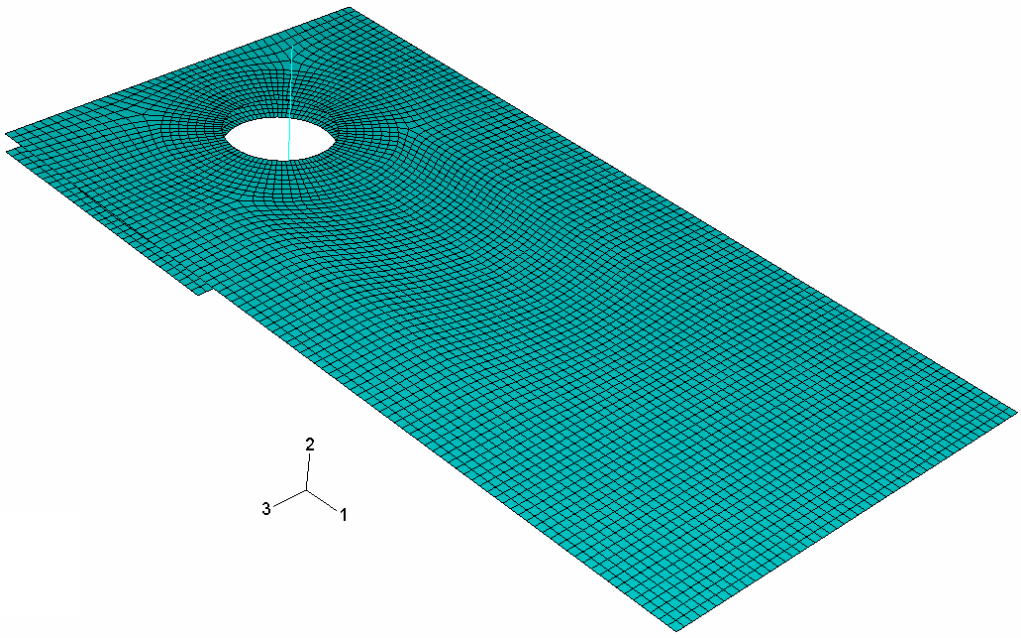

(a)

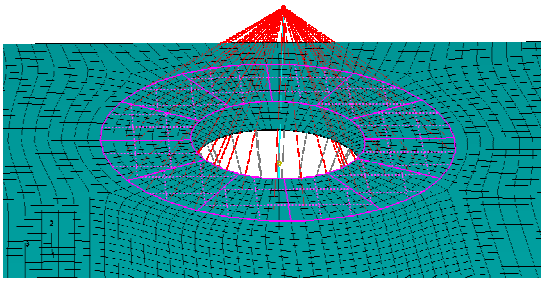

(b)

Figure 5.5 Simplified Model 3 a) an overall view of mesh pattern of the whole model b) an enlarged and marked view of coupling constraints on the model

Only contact pairs 1 and 2 which are between the frame and the plate, and between the plate and impactor, were introduced in this model.

5.4. Simplified Model 4: Timeshenko Beam-Coupling Constraint without Hole

In this model, the frame and the plate do not have bolt holes. The other features of the model are the same as the previous one. Ignoring the holes reduces the complexity in the models of the sheets. Besides, existence of the material instead of holes may simulate the effect of contact between the bolt shank and the perimeter of holes.

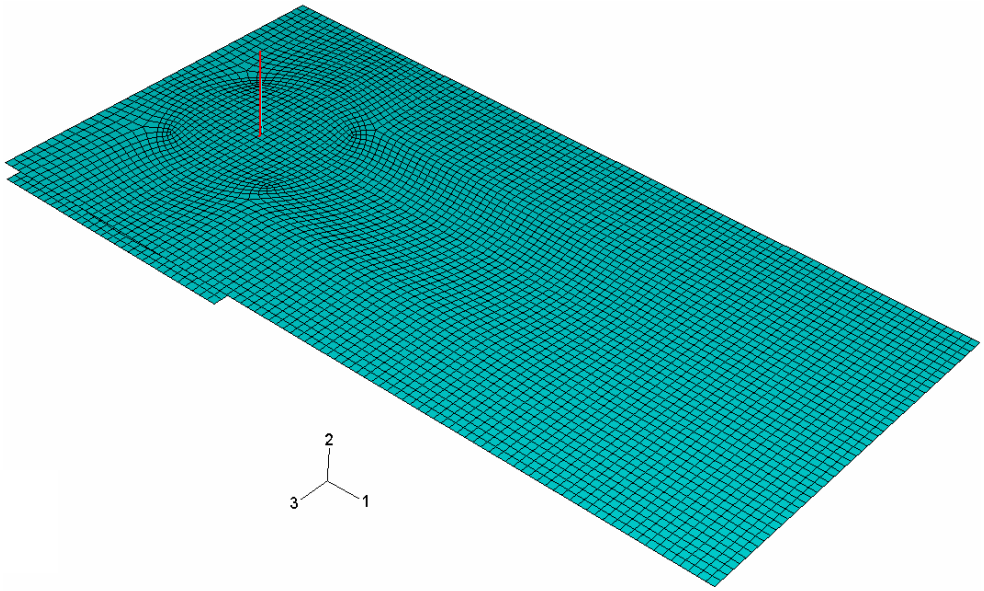

(a)

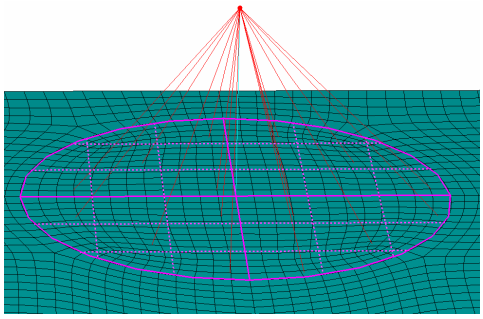

(b)

Figure 5.6 Simplified Model 4 a) an overall view of mesh pattern of the whole model b) an enlarged view of coupling constraints on the model

5.5. Simplified Model 5: Vertical Connector Beams on the Perimeter

In this model, as can be seen from Figure 5.7., twelve vertical connector beam type elements are defined, each between the two corresponding nodes of the plate and the frame to provide a rigid connection between the two sheets. They are positioned on the

perimeters of the bolt holes so as to transmit the impact forces from the plate to the frame. Considering that the sheets are thin in comparison to the bolt diameter, bolt-nut may be assumed to be non-deformable. Relative motion between the sheets may be assumed to be completely prevented through the clamping pressure of the bolted joint. Accordingly, rigid connectors prevent relative motion at the perimeters. Figure 5.8 shows that the force transmitting mechanism of the connector element (beam type) used in this model.

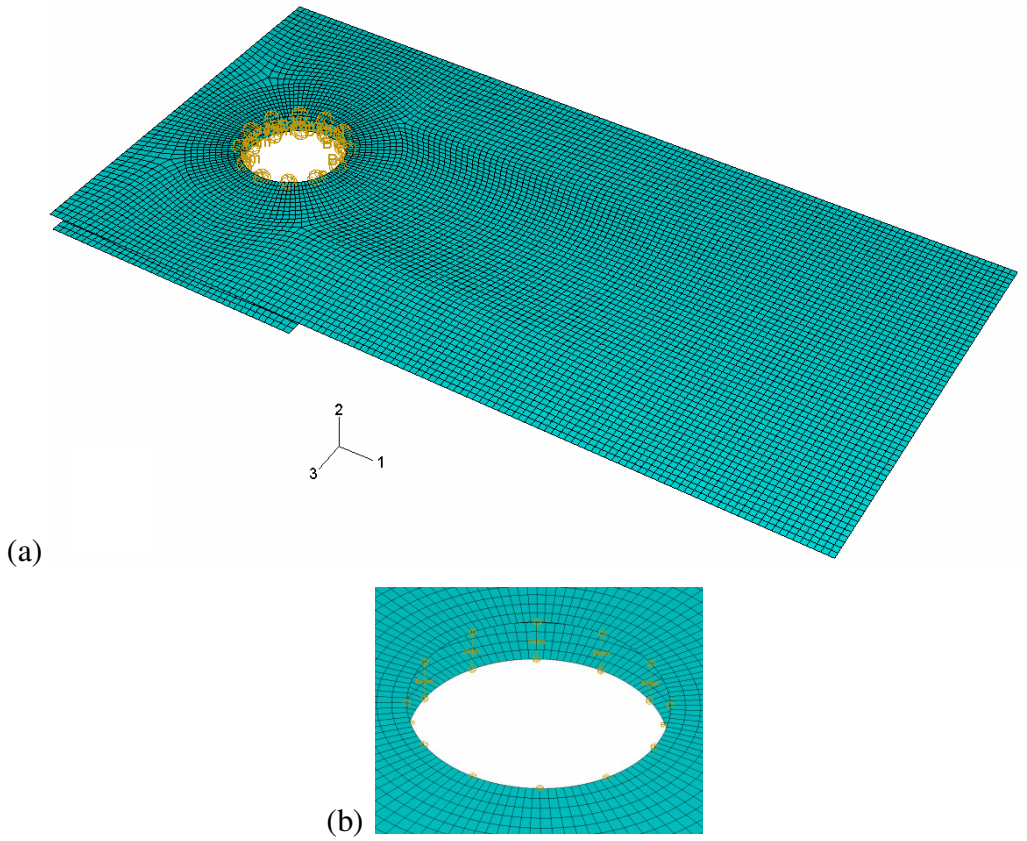

Figure 5.7 Simplified model 5 a) an overall view of mesh pattern of the whole model b) an enlarged view of connector elements on the model

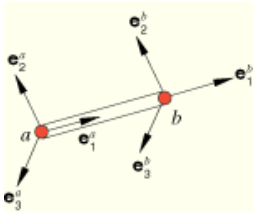

Figure 5.8 Connector beam type element

5.6. Simplified Model 6: Vertical Connector Beams on the Perimeter and the Washer Outer Line

The only difference between this model and the previous one is the additional restrained circular region. Twelve more connector beam elements are used to connect the frame and the plate along the projection line of the outer circular edge of the washer (Figure 5.9). Therefore, relative motion is prevented at more locations around the bolt hole.

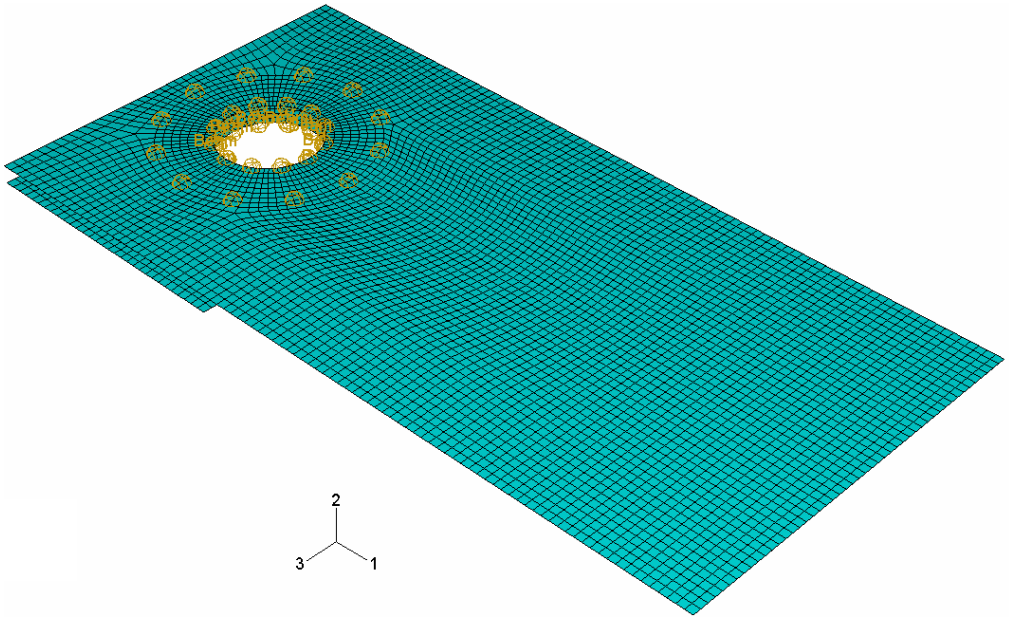

(a)

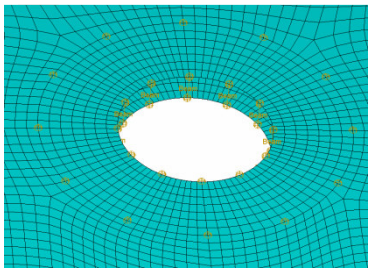

(b)

Figure 5.9. Simplified Model 6 a) an overall view of mesh pattern of the whole model b) an enlarged view of connector elements on the model

5.7. Simplified Model 7: Tie Constraint with Hole

In this model, relative motion between the sheets is prevented by defining tie constraints between the inner surfaces of the sheets within the region compressed by the washers (Figure 5.10). Force transfer between the frame and the plate is achieved through

the tie constraint. A tie constraint can be used to make the translational and rotational motions in all active degrees of freedom the same for two surfaces.

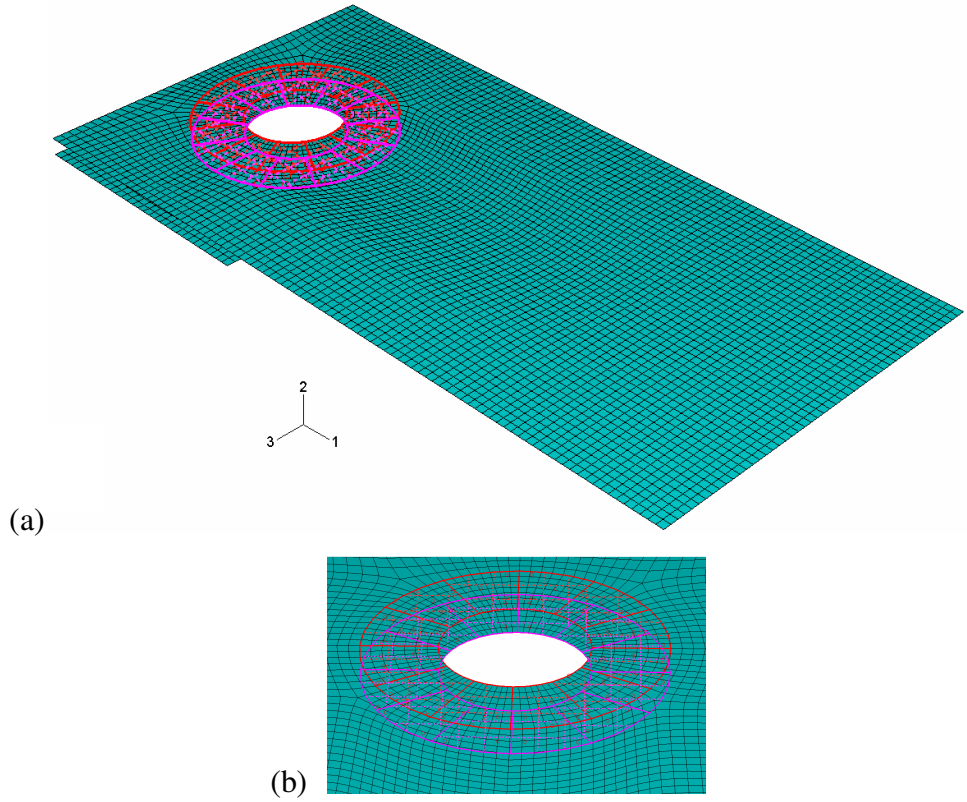

(a)

(b)

Figure 5.10. Simplified model 7 a) an overall view of mesh pattern of the whole model b) an enlarged view of tie constraints on the model

5.8. Simplified Model 8: Tie Constraint without Hole

This model also uses a tie constraint in order to model the clamping effect of the bolt-nut assembly as in the previous one, but there is no hole in this case (Figure 5.11). The tie constraint is established between the inner surfaces of the sheets within the circular region pressed by the washers. The relative distance between the plate and the frame in this region during the impact is thus kept constant via this constraint.

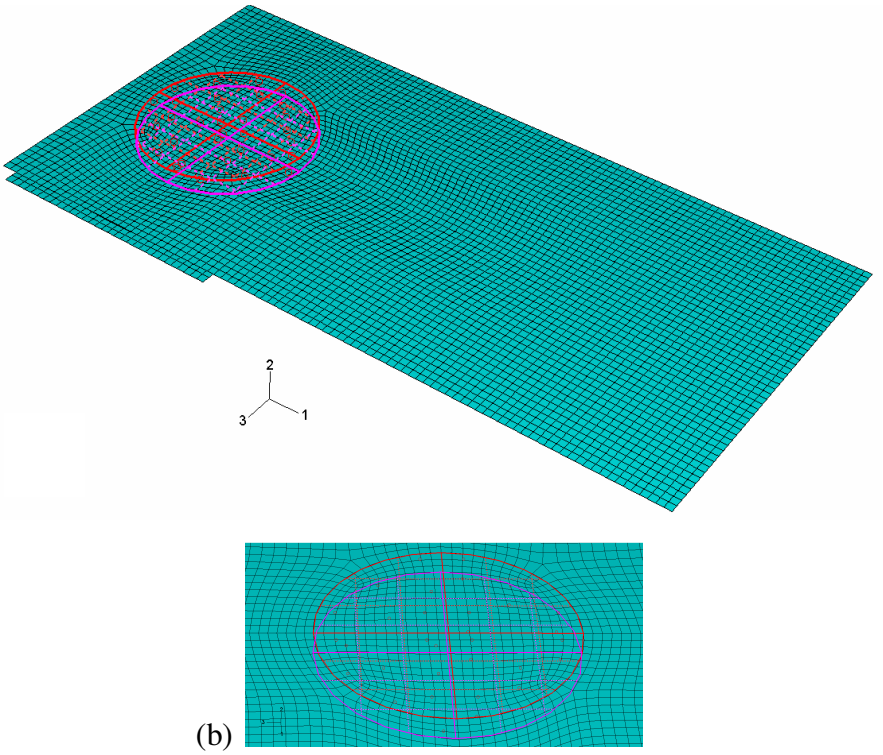

(a)

(b)

Figure 5.11. Simplified Model 8 a) an overall view of mesh pattern of the whole model b) enlarged and marked view of tie constraints on the model

5.9. Simplified Model 9: Single Connector Beam

In this model, there is no hole in the sheets. Only a single connector beam is employed so as to model the bolted joint (Figure 5.12). The connector beam element connects the corresponding nodes on the frame and on the plate located at the center of the bolt shank. Only contact pairs 1 and 2 are introduced in this model.

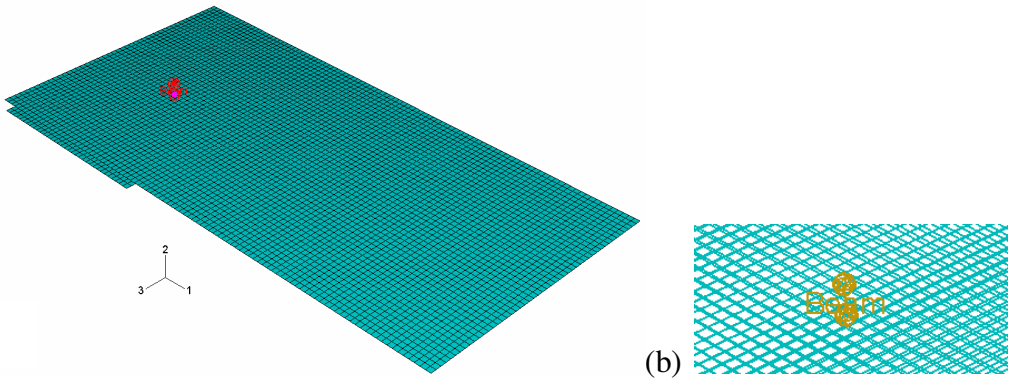

(a) (b)

Figure 5.12. Simplified model 9 a) an overall view of mesh pattern of the whole model b) an enlarged and marked view of connector element on the model

5.10. Simplified Model 10: Cross Connector Beams

In this model, there are twelve connector beam type elements that initiate from the midway of the distance between the centers of the two holes and reach to the nodes at the perimeters. Six of the connector elements are connected to the plate and the rest were connected to the frame. Its geometry and mesh structure are shown in Figure 5.13. Only contact pairs 1 and 2 are introduced in this model.

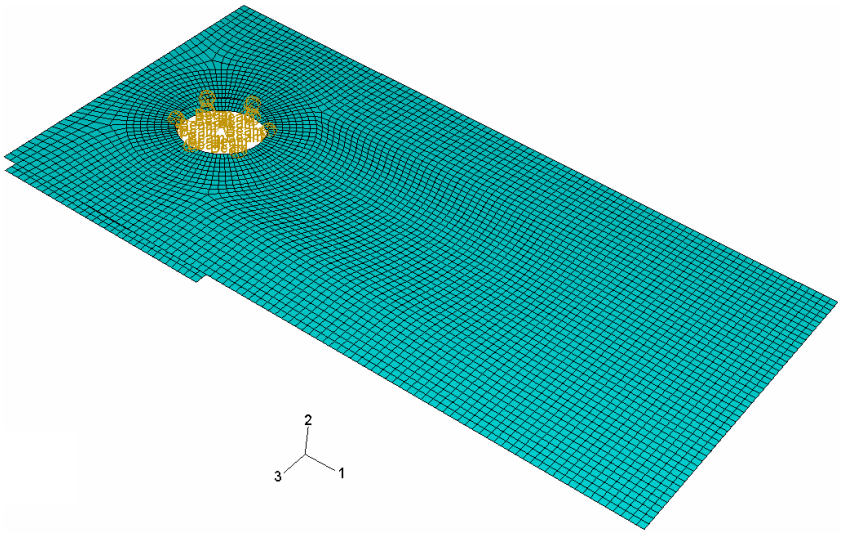

(a)

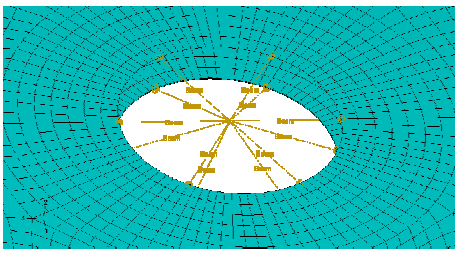

(b)

Figure 5.13 Simplified model 10 a) an overall view of mesh pattern of the whole model b) an enlarged view of connector elements on the model

5.11. Simplified Model 11: Rigid Shell Bolt

In this model, the bolt-nut assembly is modeled using shell elements with rigid material properties. Its geometry and mesh structure are shown in Figure 5.14. The flat portions of the model simulate the restrictive effect of the washers. Because of the restraining effect of the bolt head and nut, the washers are assumed not to bend. The bolt shank is also assumed to be non-deformable. The contact pairs 1, 2, 9, and 10 are

introduced in this model. In this way, the effect of contact between the bolt shank and the sheets is accounted for.

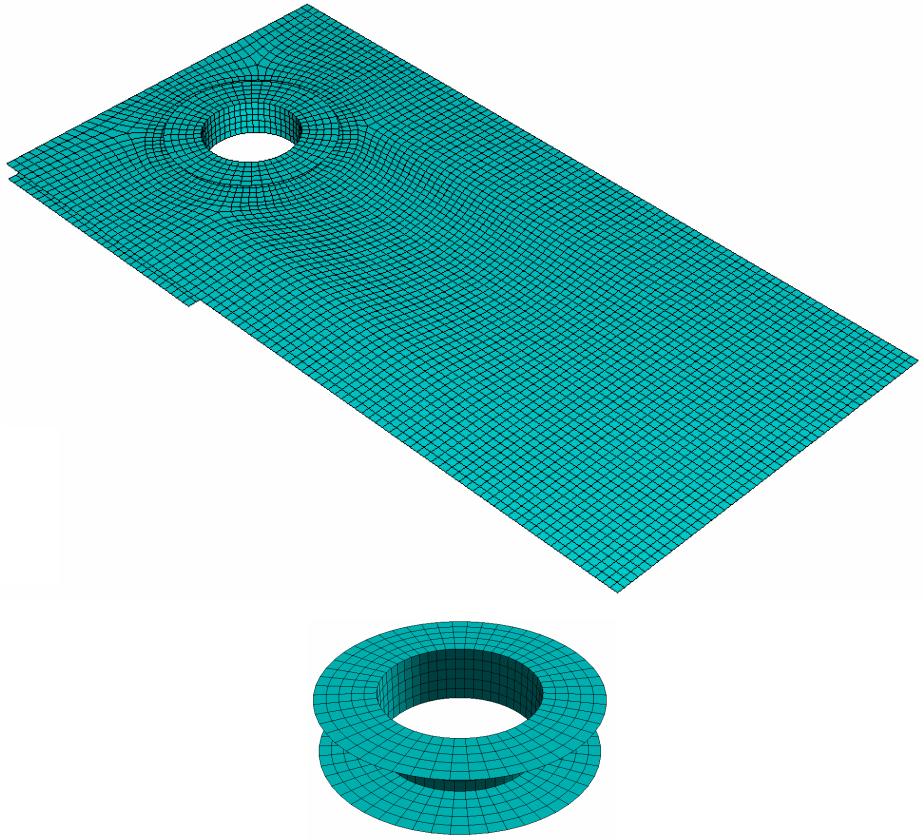

Figure 5.14 Simplified model 11 a) an overall view of mesh pattern of the whole model b) an enlarged view of simplified bolt model

5.12. Simplified Model 12: Cross Coupling Constraint

In this model, solely one coupling constraint is applied so as to simulate the effect of the bolt. This time, kinematic coupling constraint is employed. At the center of the bolt hole, there is a control point that handles the one coupling constraint with two distinct surfaces, since one control point can only manage one coupling constraint. Kinematic coupling constraint used here coupled all degrees of the freedom of nodes on the surfaces to the control point. Only contact pairs 1 and 2 are introduced in this model.

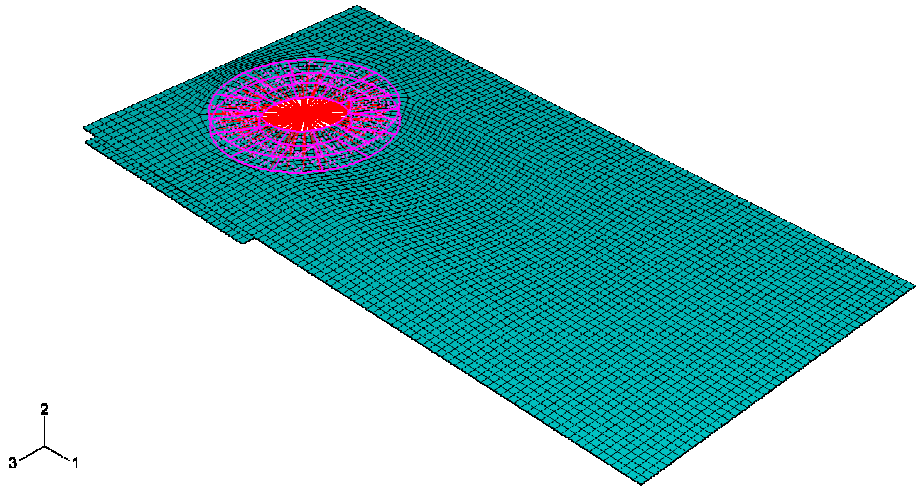

Figure 5.15 Simplified model 12

5.13. Simplified Model 13: Deformable Shell Bolt

Apart from the simplified model 11 the bolt-nut assembly is modeled using shell elements with deformable material properties. In this model, the shell has a thickness of 0.25 mm. In order to make the elasticity modulus times moment of inertia the same for the full bolt model, the formula of

is used. Thus, the elasticity modulus used in this model is 900 GPa.

6. RESULTS AND DISCUSSION

In this study, a number of finite element analyses were carried out in order to predict stress and strain distributions in the sheets fastened by bolted joints. At first, convergence analyses were conducted for the full bolt model and the simplified models with respect to element size. The results of the full model were used as the benchmark to test the accuracy of the simplified models. Then, the simplified models were compared as to the accuracy, solution time and difficulty in modeling.

After the completion of a number of analyses, it was observed that the total CPU run time to complete each individual model was ranging from a few minutes to about a couple hours with Intel(R) Xeon(R) CPU E5410 @233 GHz 4,00 GB of RAM depending on the mesh refinement and model complexity.

6.1. Validation of the Solution

Since the finite element method is an approximate solution technique, one should ensure that the resulting error is less than an acceptable limit. The finite element software guides the user by issuing some warning massages for some mistakes the user makes in the modeling. However, one should not completely rely on these massages. One of the ways to check the accuracy of the results is the mesh-convergence analysis. One should determine the range of values for the mesh size for which one can obtain consistent results. Energy output is another indication for the validity of an explicit analysis. Comparisons between various energy components can be used to help evaluate whether an analysis has yielded an acceptable response.

6.1.1. Examination of the Energy Outputs

The energy balance for the entire system can be written as

$$E_I + E_V + E_{FD} + E_{KE} - E_W = E_{total} = constant \tag{6.1}$$

where E_I is the internal energy, E_V is the viscous energy dissipated, E_{FD} is the frictional energy dissipated, E_{KE} is the kinetic energy, and E_W is the work done by the externally applied loads. The sum of these energy components for both the impactor and the sheets is E_{total}, which should be constant. In a numerical analysis E_{total} is only approximately constant, generally with an error of less than 1.0% [23]

The internal energy is the sum of the recoverable elastic strain energy, E_E, the energy dissipated through inelastic processes such as plasticity, E_P, the energy dissipated through visco-elasticity or creep, E_{CD}, and the artificial strain energy, E_A.

The artificial strain energy includes the energy stored in hourglass resistances and transverse shearing in shell and beam elements. Large values of artificial strain energy indicate that improvement in the mesh is necessary.

Firstly, consider the kinetic energy histories of the full model for the two configurations. At the beginning of the simulation the impactor is in free fall, and the energy is totally in the form of kinetic energy. During the initial stages of impact, mechanical energy is transferred to the plate, resulting in the deformation of the sheets, and increase in the internal energy and reduction in the kinetic energy. The sheets then deflect while restrained at the sides until the middle of the plate reaches its maximum deflection. After that, the impactor bounces back leading to increase in the kinetic energy. Because in configuration 2, impact load is more severe, energy associated with plastic deformation is much larger in comparison to the elastic energy.

From Figures 6.1 and 6.2, one can see that the internal energy increases as the kinetic energy decreases. The internal energy is composed of elastic energy and plastically dissipated energy, both of which are also plotted in these figures. Elastic energy rises to a peak and then falls as the elastic deformation recovers during the upward movement of the impactor, but the plastically dissipated energy continues to rise because this energy cannot be recovered.

Another important energy output is the artificial energy. Usually it should be held to a small fraction of the internal energy to keep the error low, because hourglass energy does

not correspond to any physical process; it is only introduced to overcome numerical difficulties associated with excessive deformation. In the analyses of this study, the artificial energy of the system is a small fraction of the internal energy as can be seen in the Figures 6.1-14. The total energy remains constant during the simulations for all of the models.

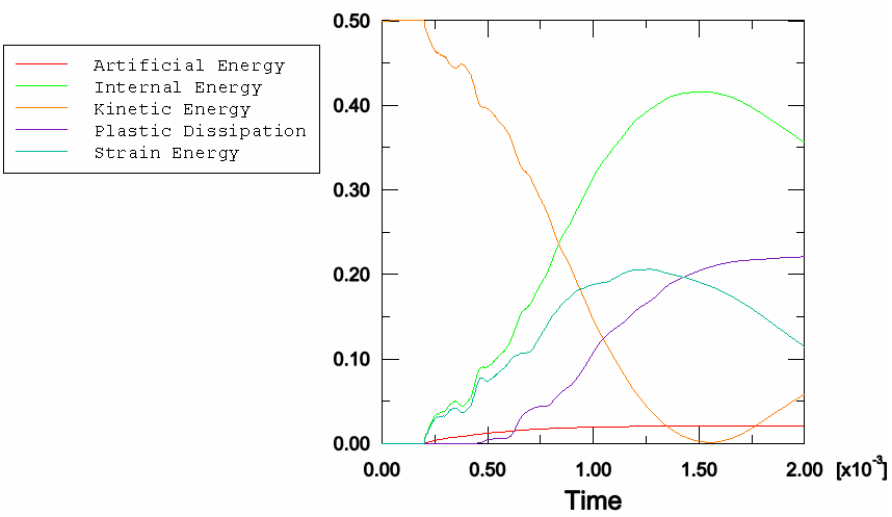

Figure 6.1. Energy results versus time for the full model with a mesh seed of 0.66 mm for configuration 1

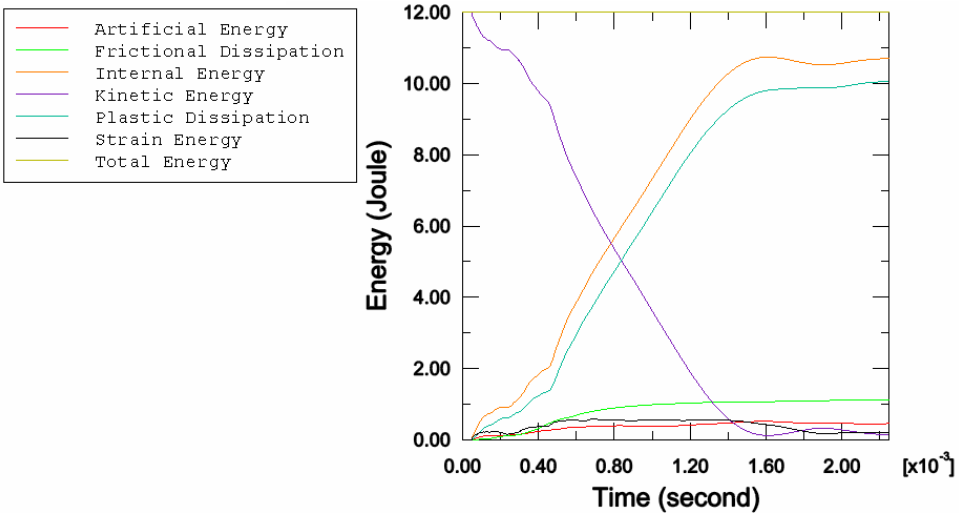

Figure 6.2. Energy results versus time for the full model with a mesh seed of 0.66 mm for configuration 2

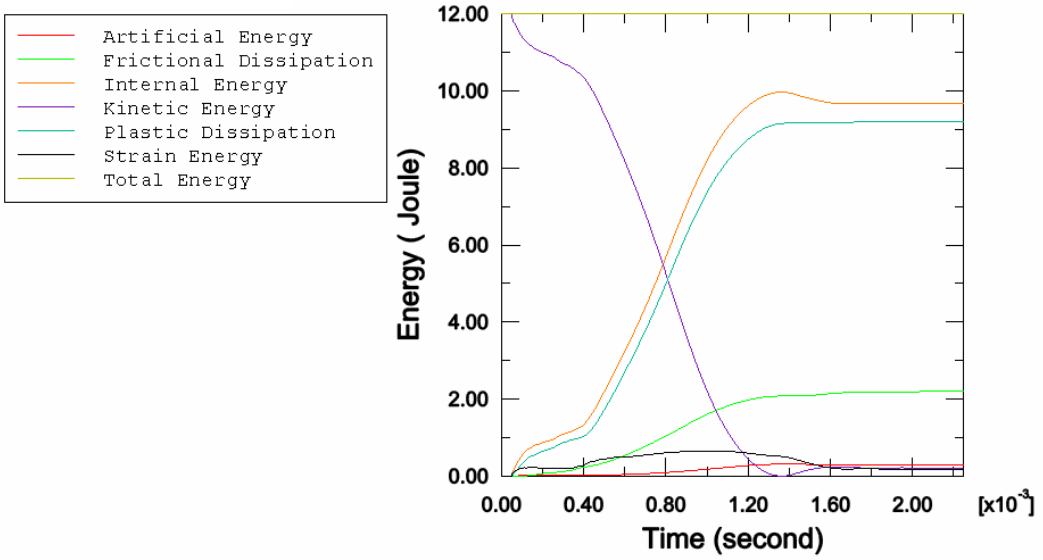

Figure 6.3. Energy results versus time for the simplified model 1 with a mesh seed of 0.66 mm for configuration 2

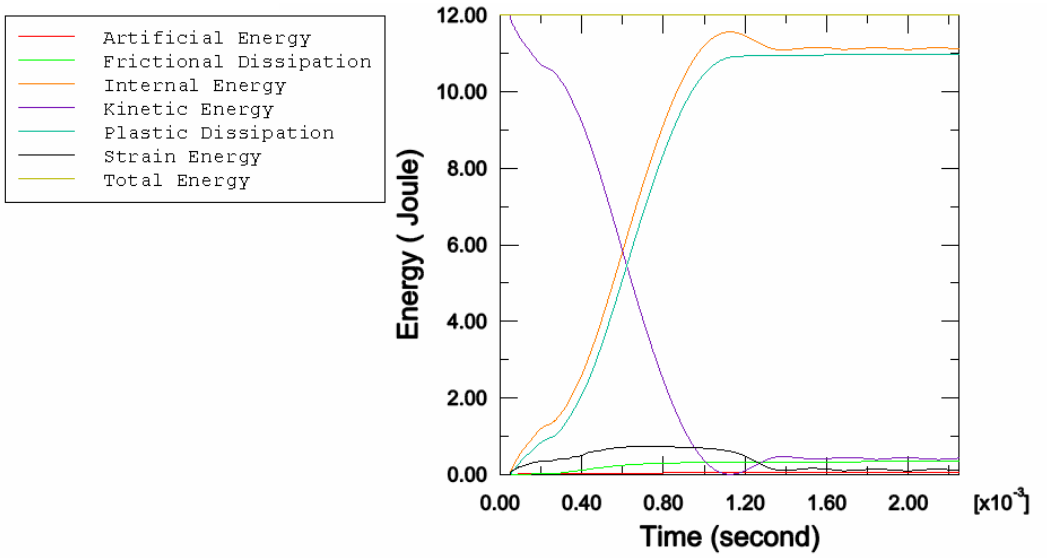

Figure 6.4. Energy results versus time for the simplified model 2 with a mesh seed of 0.66 mm for configuration 2

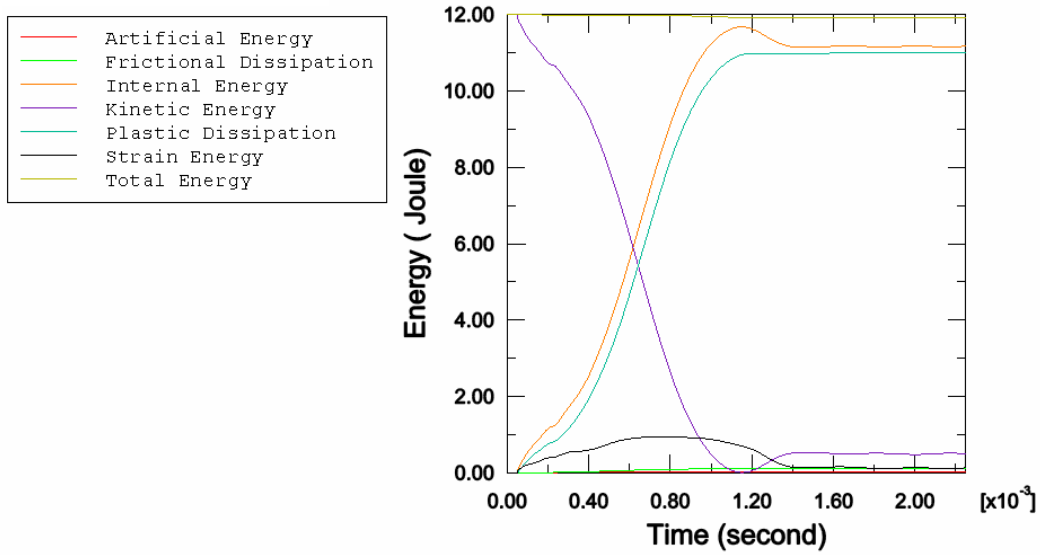

Figure 6.5. Energy results versus time for the simplified model 3 with a mesh seed of 0.66 mm for configuration 2

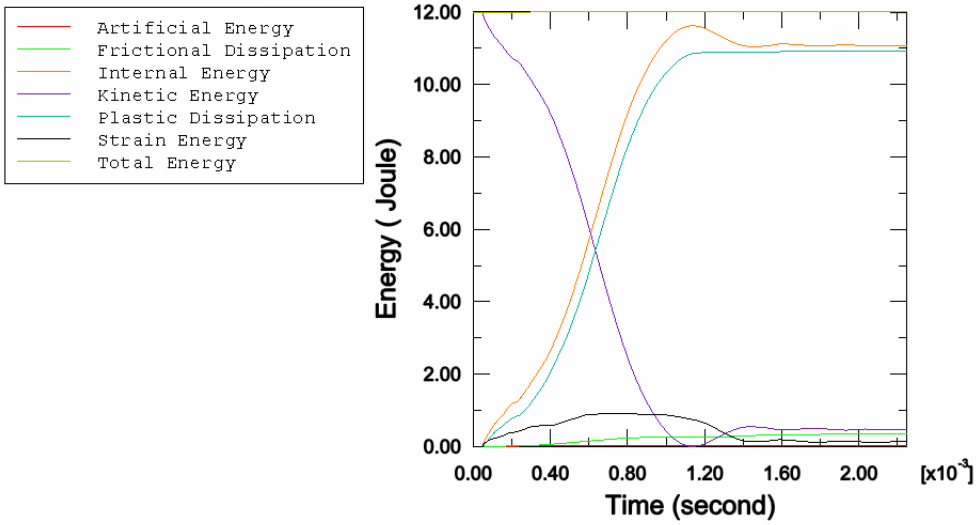

Figure 6.6. Energy results versus time for the simplified model 4 with a mesh seed of 0.66 mm for configuration 2

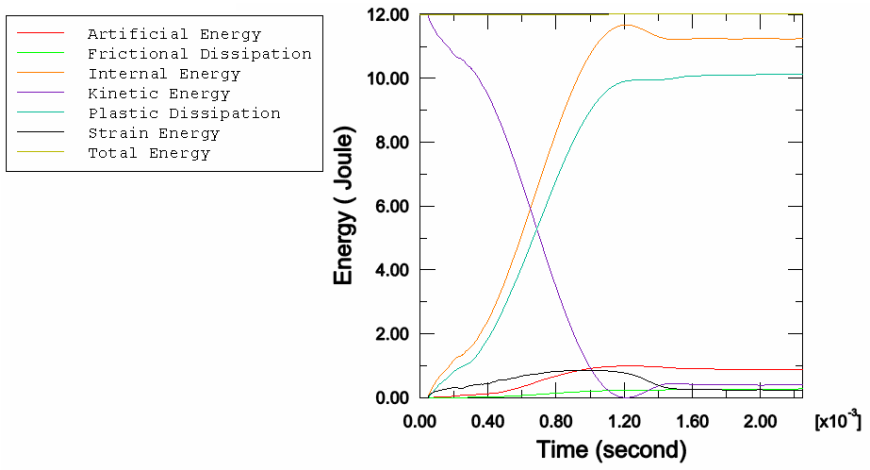

Figure 6.7. Energy results versus time for the simplified model 5 with a mesh seed of 0.66 mm for configuration 2

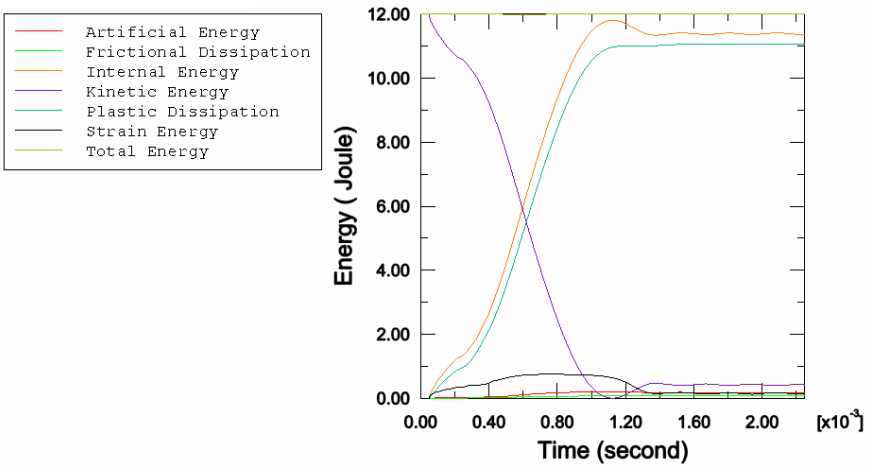

Figure 6.8 Energy results versus time for the simplified model 6 with a mesh seed of 0.66 mm for configuration 2

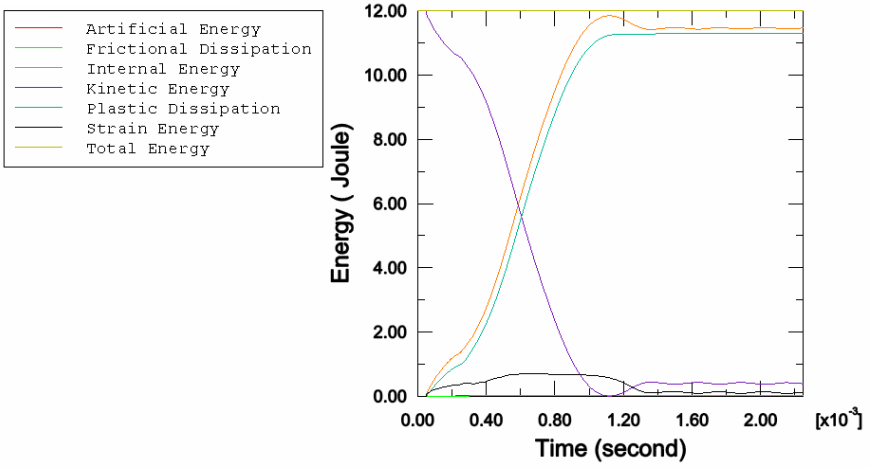

Figure 6.9 Energy results versus time for the simplified model 7 with a mesh seed of 0.66 mm for configuration 2

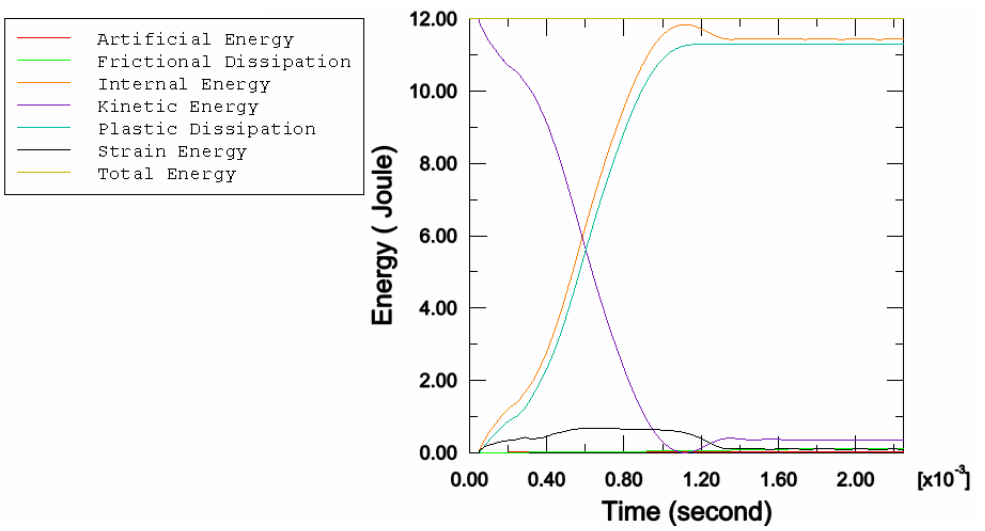

Figure 6.10. Energy results versus time for the simplified model 8 with a mesh seed of 0.66 mm at configuration 2

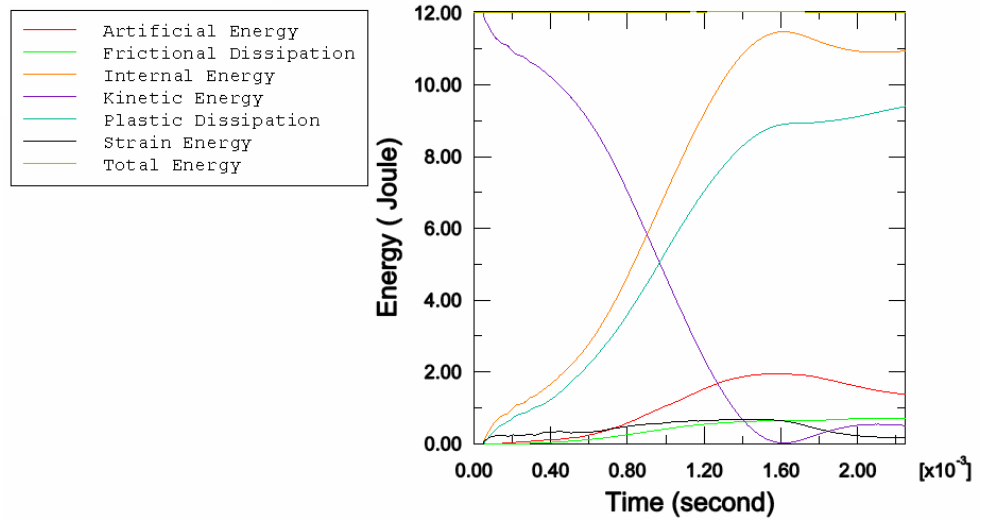

Figure 6.11. Energy results versus time for the simplified model 9 with a mesh seed of 0.66 mm for configuration 2

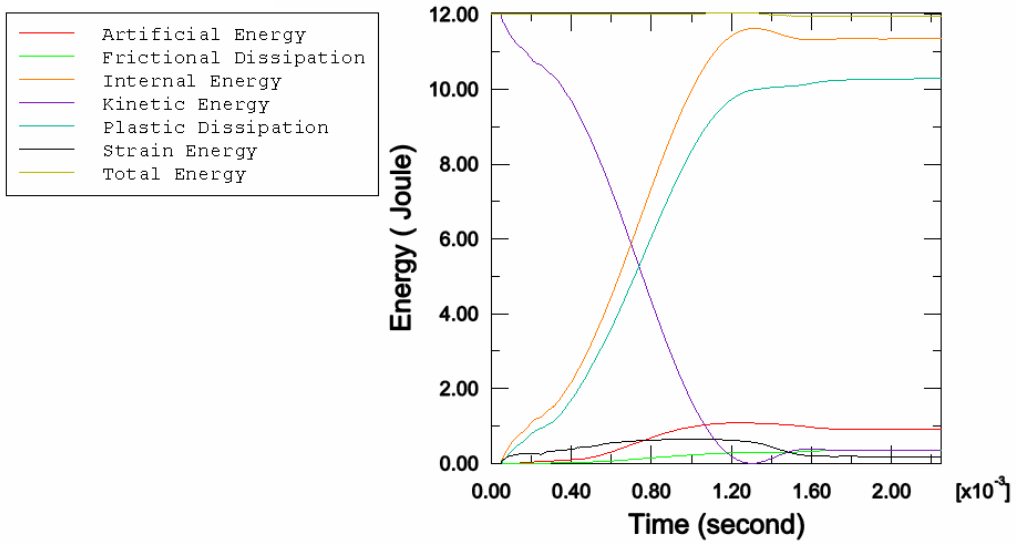

Figure 6.12. Energy results versus time for the simplified model 10 with a mesh seed of 0.66 mm for configuration 2

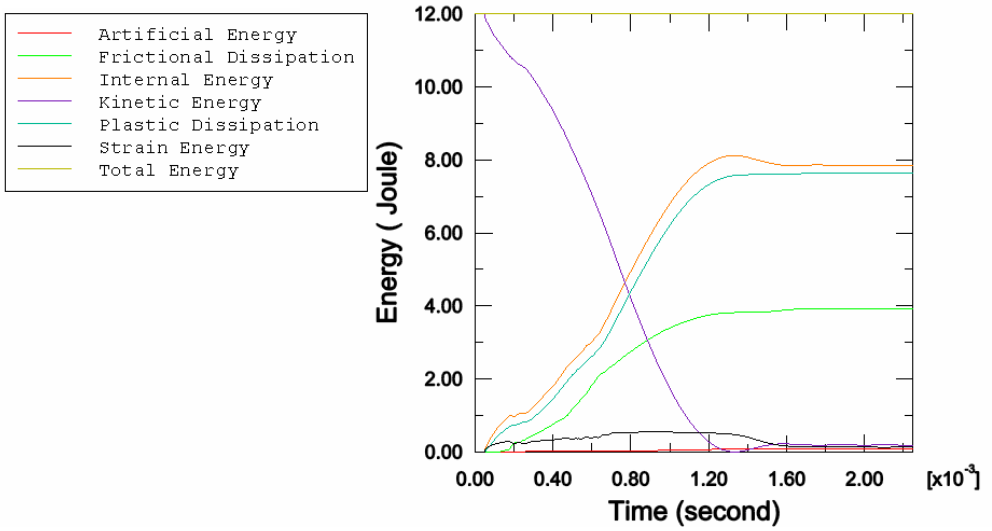

Figure 6.13. Energy results versus time for the simplified model 11 with a mesh seed of 0.66 mm for configuration 2

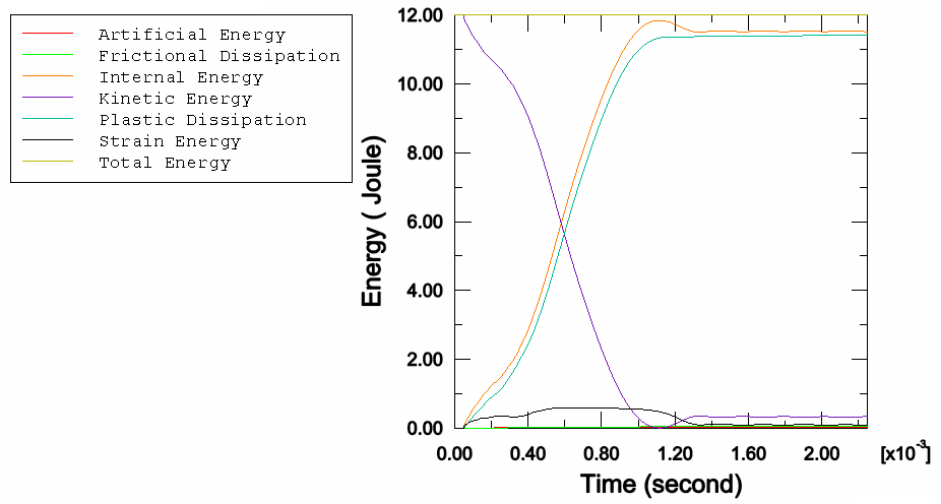

Figure 6.14. Energy results versus time for the simplified model 12 with a mesh seed of 0.66 mm for configuration 2

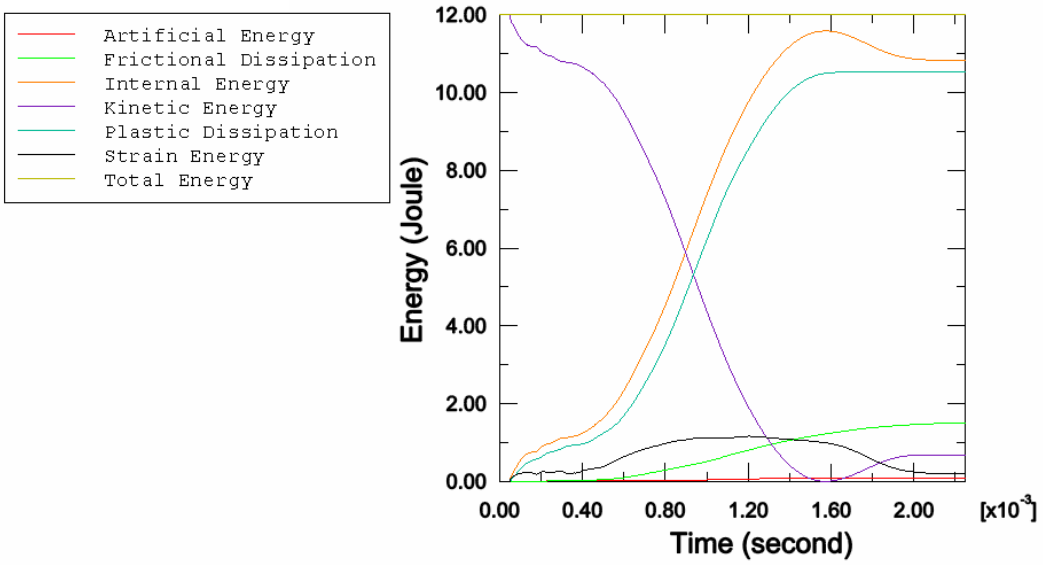

Figure 6.15. Energy results versus time for the simplified model 13 with a mesh seed of 0.66 mm at configuration 2

6.1.2. Convergence Analysis for the Full Model

Since the finite element method is an approximate solution technique, one should ensure that the resulting error is less than an acceptable limit. The finite element software guides the user by issuing some warning massages for some mistakes the user makes in the modeling. However, one should not completely rely on these massages. One of the ways to check the accuracy of the results is the mesh-convergence analysis. One should determine the range of values for the mesh size for which one can obtain consistent results.

In this work, the maximum plastic strain and von Mises stress around the bolt hole and near the middle region of the plate (see Figures 6.16 and 6.17) and the maximum deflection were chosen as control parameters. In order to find the optimum value of the element size, a number of analyses were carried out for element sizes 2.0, 1.0, 0.66, and 0.5 mm; but the dimensions of the brick elements in the thickness direction were equal to the half of these values. Tables 6.1-6 and Figures 6.18-19 show the results for the chosen element sizes.

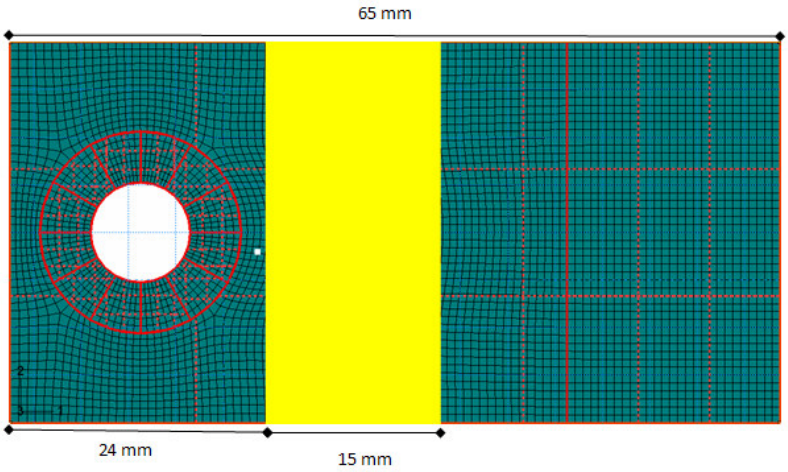

Figure 6.16. Middle region of the plate used for stress-strain comparisons for configuration 1

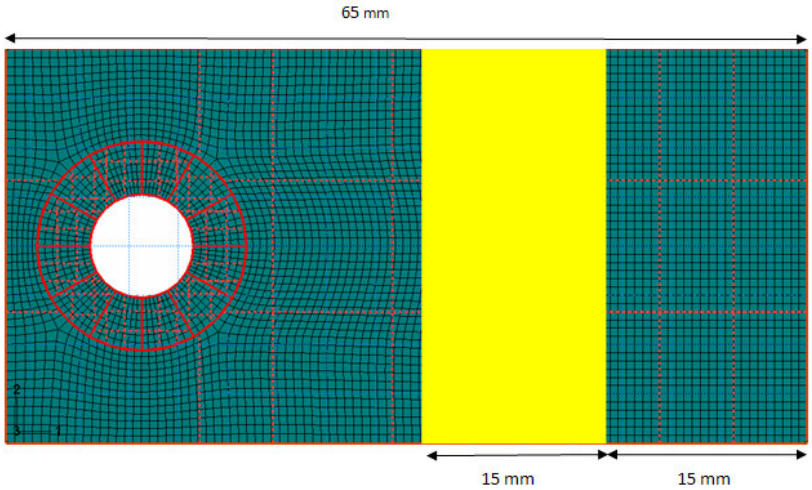

Figure 6.17. Middle region of the plate used for stress-strain comparisons for configuration 2

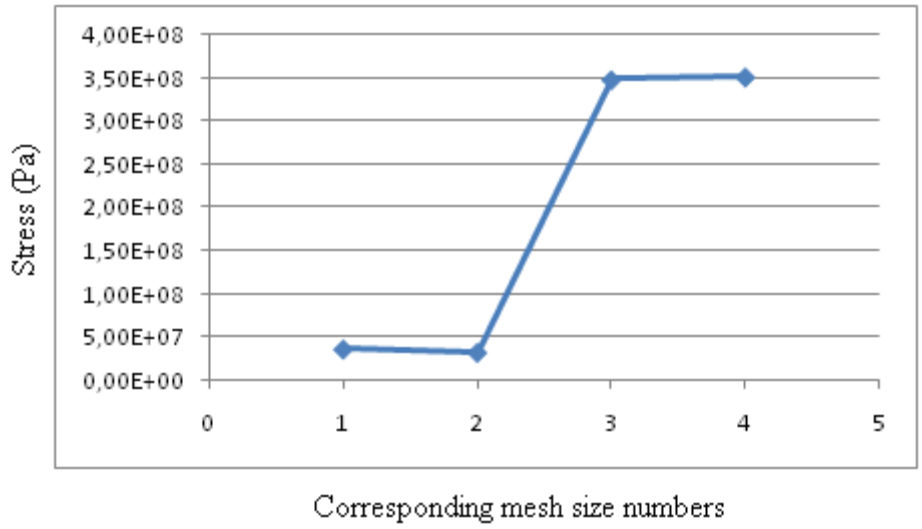

Figure 6.18. Maximum von Mises stress in the full model obtained with different mesh sizes for configuration 1

Table 6.1.Analysis times of the models for configuration 1

Model Name config-1	Mesh Size (mm)	Analysis Time (s)	Analysis Time Normalized
Full Model	0.5	59980	336.4
	0.66	17831	100.0
	1.0	2503	14.0
	2.0	284	1.6

Table 6.2. Maximum von Mises stress in the middle zone of the sheet for configuration 1

Model Name configuration 1	Mesh Size (mm)	Max. von Mises At Middle zone (MPa)	Normalized
Full Model	0.5	351	100.9
	0.66	348	100.0
	1.0	331	9.5
	2.0	370	10.6

Table 6.3.Central displacements of full model for configuration 1

Model Name configuration 1	Mesh Size (mm)	Center Displacement (mm)	Center Displacement Normalized
Full Model	0.5	-3.76915	98.8
	0.66	-3.81385	100.0
	1.0	-3.85152	101.0
	2.0	-7.10257	186.2

In the full model, through the thickness of the plate there are 1, 2, 3, and 4 elements corresponding to mesh sizes of 2.0 mm, 1.0 mm, 0.66 mm, and 0.5 mm, respectively. The poor performance of the models with mesh sizes of 2.0 mm and 1.0 mm may be attributed to low number of elements through the thickness. However, one may assume that 0.66 mm mesh size is sufficiently small for obtaining convergence. For the high loading case (configuration 2) even 1.0 mm mesh size yields acceptable results.

In order to preload the bolt, an artificial orthotropic coefficient of thermal expansion was defined for one of the washers. This artificial coefficient induces the washer expansion only in the axial direction with temperature increase. In this way, the bolt can be tensioned to desired preload, %80, of its yield strength of 220 MPa. The temperature difference introduced to the washer was 85°C. The initial temperature is 0°C. The artificial coefficient thermal expansion is 9.616E-05 m/m/°C.

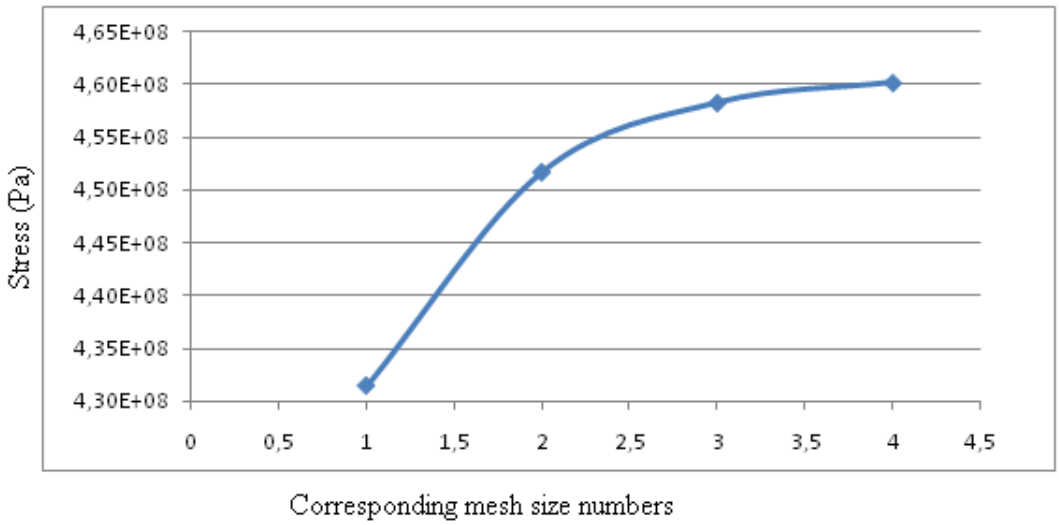

Figure 6.19. Maximum von Mises stress in the full model obtained with different mesh densities for configuration 2

Table 6.4. Analysis times of the models for configuration 2

Model Name	Mesh Size (mm)	Analysis Time (s)	Analysis Time Normalized
Full Model	0.5	59183	315.9
	0.66	18735	100.0
	1.0	2448	13.1
	2.0	247	1.3

Table 6.5. Maximum von Mises stress around the bolt hole of the full model for configuration 2

Model Name	Mesh Size (mm)	Von Mises Stress around The Hole on Plate (MPa)	Von Mises Stress Normalized
Full Model	0.5	4.60	100.4
	0.66	4.58	100.0
	1.0	4,52	98.6
	2.0	4,31	94,2

Table 6.6. Maximum plastic strain around the bolt hole of full model for configuration 2

Model Name	Mesh Size (mm)	Max. Plastic Strain Around Hole on Plate	M P. Strain Normalized
Full Model	0.5	0.113854	113.2
	0.66	0.100572	100.0
	1.0	0.0963535	95.8
	2.0	0.0397501	39.5

Table 6.7. Central deflection of the full model for configuration 2

Model Name	Mesh Size (mm)	Center Displacement (m)	Center Displacement Normalized
Full Model	0.5	-0.01514	101.0
	0.66	-0.01499	100.0
	1.0	-0.01513	101.0
	2.0	-0.01342	89.5

The results were also obtained by including pretension. As seen in Table 6.?, smaller plastic strains were obtained near the bolt hole as expected. The stresses, on the other hand, are lower for configuration 1, but about the same for configuration 2. As for the central displacement, it is a slightly lower.

Table 6.8. The results of the full model with pre-tension of configuration 1

Plastic Strain Around Hole	Stress Around The Hole (MPa)	Plastic Strain at Middle Zone	Stress at Middle Zone (MPa)	Center Displacement (mm)
0.00	221	0.000215107	262	-3.22
0.00	192	0.0011541	328	-3.28
0.00	159	0.00	71.2	-4.49

Table 6.9. The results of the full model with pre-tension of configuration 2

Plastic Strain Around Hole	Stress Around The Hole (MPa)	Stress at Middle Zone (MPa)	Plastic Strain at Middle Zone	Center Displacement (mm)
0.0898865	457	414	0.00308403	-14.62
0.0854923	450	422	0.00341088	-14.53
0.0622706	442	404	0.00411813	-14.32
0.032572	396	301	9.47254E-005	-13.04

In the pre-tensioned analysis, there is a decrease in the plastic strains near the bolt as can be predicted. But the stresses around the bolt hole are almost the same. A careful observation reveals that at the center displacement of the whole set-up there is a slight decrease as well.

6.3. Comparison of the Numerical and Analytical Results

One may idealize the structure as a linear elastic beam fixed at both ends and subjected to an impact load at its middle. This beam's center deflection can then be calculated analytically. Firstly, the static deflection is calculated that is induced by a point force with a magnitude being equal to the weight of the impactor in order to estimate the

impact factor. The mass of the impactor is 0.12 kg, the lengths of the plate can be considered as 0.13-2*0.0224 and 0.13-2*0.0222 m, respectively and the static deflection at the center is given by

$$\delta_{st} = \frac{WL^3}{192EI} \tag{6.2}$$

where W is the weight of the impactor, E is Young's modulus, I is the area moment of inertia. Using this formula, δ_{st} is found as $0.0595\ mm$. $0.0686\ mm$. The deflection due to the impact load is given by

$$\delta_{max} = \delta_{st}(1 + \sqrt{1 + \frac{2h}{\delta_{st}}}, \tag{6.3}$$

where h is equal to $\frac{v^2}{2g}$, v is the velocity of the striking object, g is the gravitational acceleration. Finally, the δ_{max} is found as 3.1and 16.72 mm, respectively.

6.4. Results for the Simplified Models

A careful observation of Table 6.1-3 reveals the fact that for small strain-valued impact analysis, simplified Model 9 showed better performance than the others away from the bolt holes. But its performance around the hole for strain values was poor.

Table 6.10. Normalized values of the chosen outputs for the bolt models for configuration 1

	Analysis time	Plastic Strain around hole	Von Mises Stress around hole	Plastic Strain On Middle	von Mises Stress 0n Mid.	Center Displacement
Full model	100.0	0.0	100.0	100	100.0	100.0
Simplified Model 1	228.6	0.0	130.8	32.6	106.9	95.1
Simplified Model 2	15.0	0.0	135.2	102.5	102.5	85.1
Simplified Model 3	12.4	0.0	136.8	33.4	100.4	88.8
Simplified Model 4	33.3	0.0	159.0	19.3	100.9	92.3
Simplified Model 5	10.6	0.0	183.3	291.2	99.9	92.2
Simplified Model 6	9.5	0.0	156.6	45	102.1	86.8
Simplified Model 7	14,0	0.0	157.4	47.5	102.8	84,1
Simplified Model 8	9.5	0.0	136.9	49.2	102.4	85.9
Simplified Model 9	7.7	0.0	194,0	136.4	111.6	103.3
Simplified Model 10	12.3	0.0	190.9	49.9	97.7	94,7
Simplified Model 11	14.3	0.0	130.8	32.6	100.9	76.8
Simplified Model 12	11.5	0.0	133.8	107.7	105.9	79.9

Table 6.11. Normalized values of the chosen outputs of the bolt models for configuration 2

	Analysis Time (s)	Plastic Strain Around Hole	Von Mises Stress Around Hole	Plastic Strain on The Middle	von Mises Stress on Middle zone	Center Displacement
Full model	100.0	100.0	100.0	100.0	100.0	100.0
Simplified Model 1	199.2	166.3	104,6	136.5	101.9	107.0
Simplified Model 2	16.5	48.8	93.4	773.5	99.5	86.7
Simplified Model 3	15.2	47.6	91.8	745.2	101.9	86.8
Simplified Model 4	16.2	50.8	95.0	822.6	97.8	86.2
Simplified Model 5	15.4	933.1	274.7-96.3	157.0	102.2	98.7
Simplified Model 6	12.6	133.4	104,5	979.2	102.4	86.8
Simplified Model 7	14,3	56.8	96.6	1120.3	101.6	85.9
Simplified Model 8	15.8	62.8	97.0	1048.2	101.6	85.5
Simplified Model 9	10.9	1187.8	295.7	137.5	119.2	131.0
Simplified Model 10	14,5	894,1	125.0	272.3	99.5	95.0
Simplified Model 11	17.7	139.1	104,3	138.9	95.3	98.4
Simplified Model 12	14,5	47.0	96.6	1069.4	101.7	85.3
Simplified Model 13	20.3	316.3	117.6	170.9	102.6	127.7

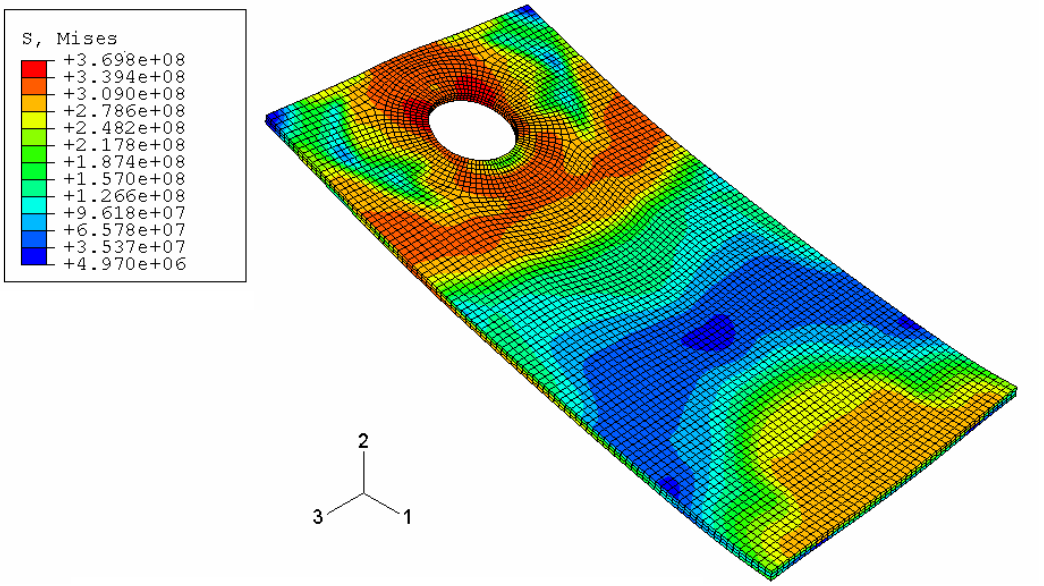

Figure 6.20. Maximum deformation of the full model at 0.001406 s

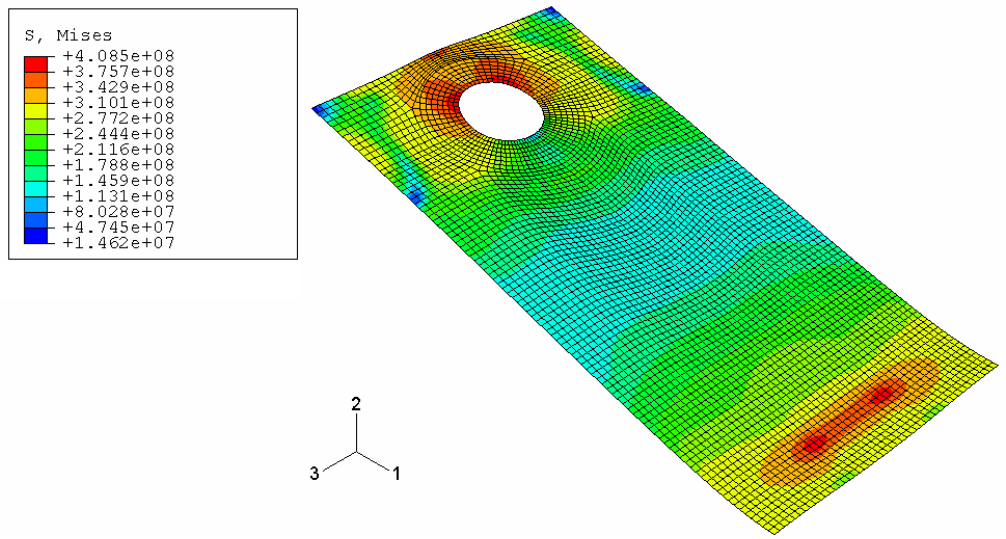

Figure 6.21. Maximum deformation of simplified model 1 at 0.00135 s

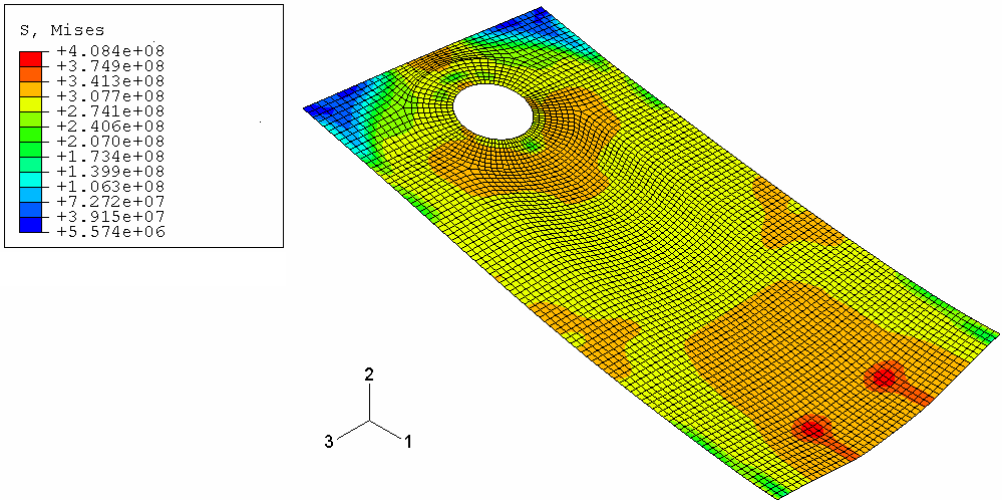

Figure 6.22. Maximum deformation of Simplified model 2 at 0.001125 s

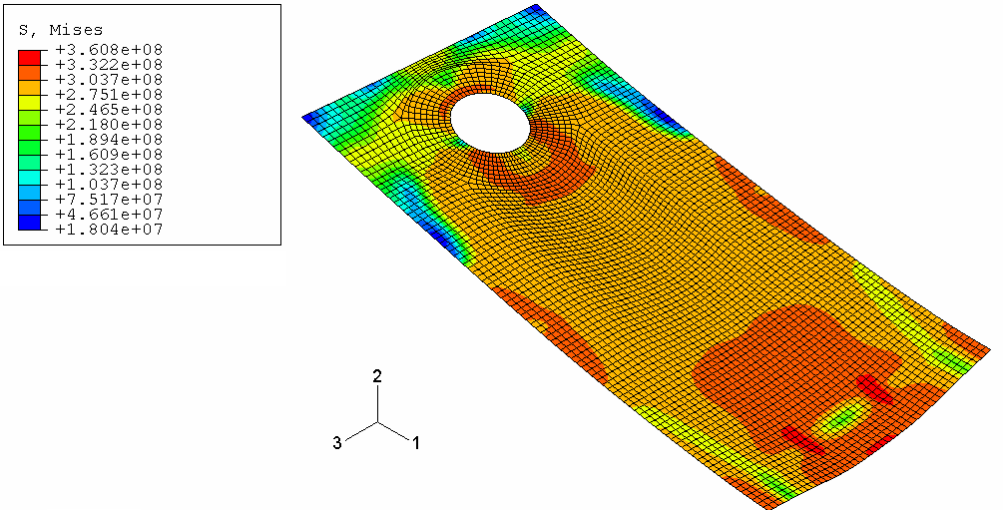

Figure 6.23. Maximum deformation of Simplified model 3 at 0.001170 s

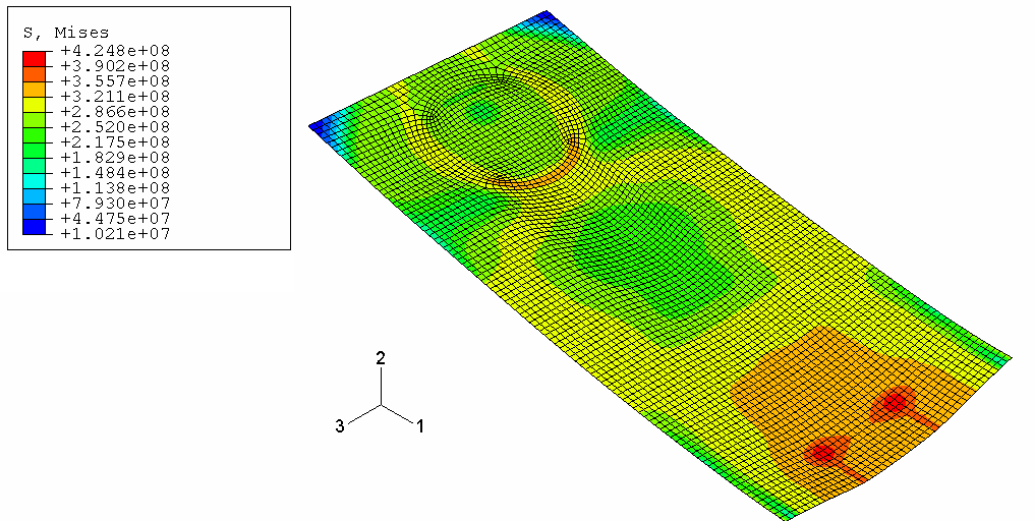

Figure 6.24. Maximum deformation of Simplified model 4 at 0.001125 s

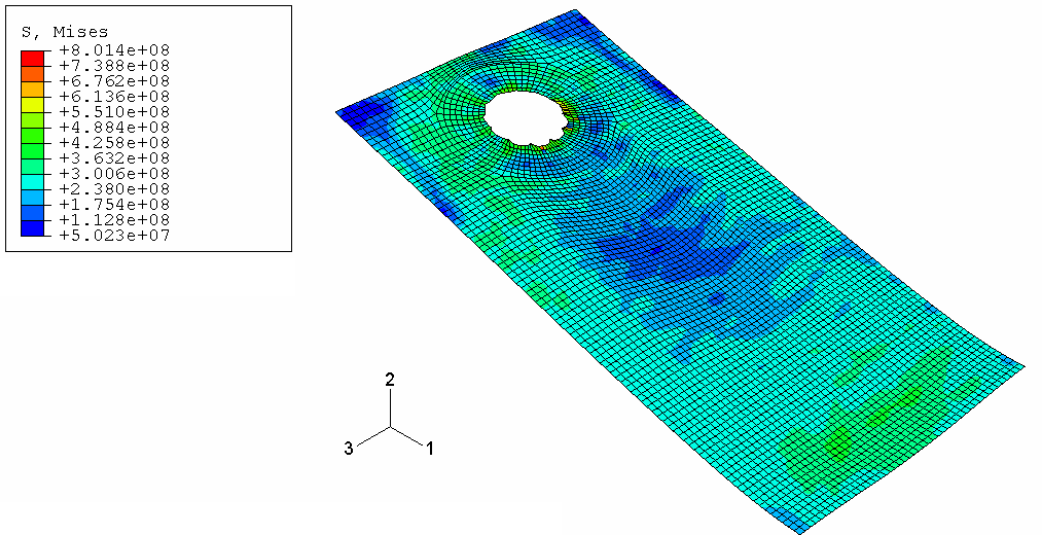

Figure 6.25. Maximum deformation of Simplified model 5 at 0.001125 s

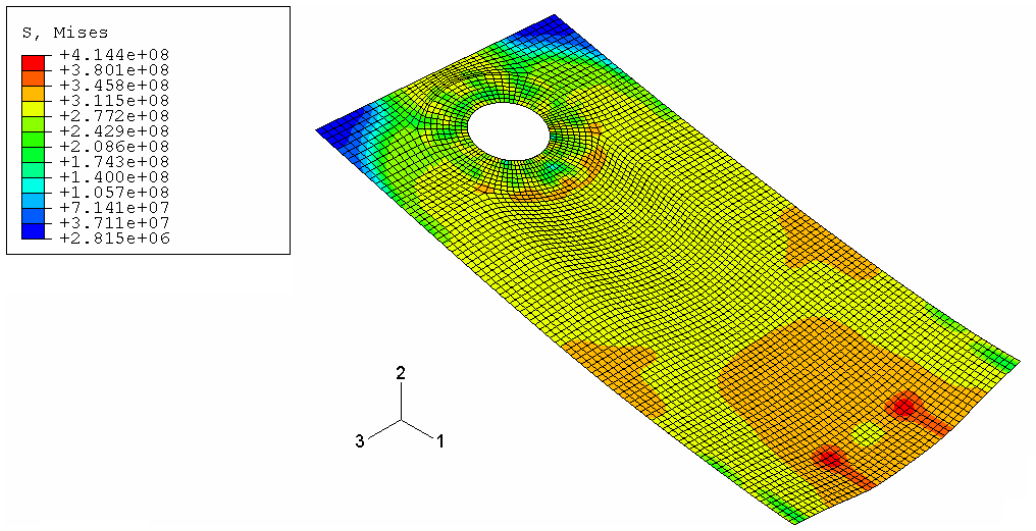

Figure 6.26. Maximum deformation of Simplified model 6 at 0.0012825 s

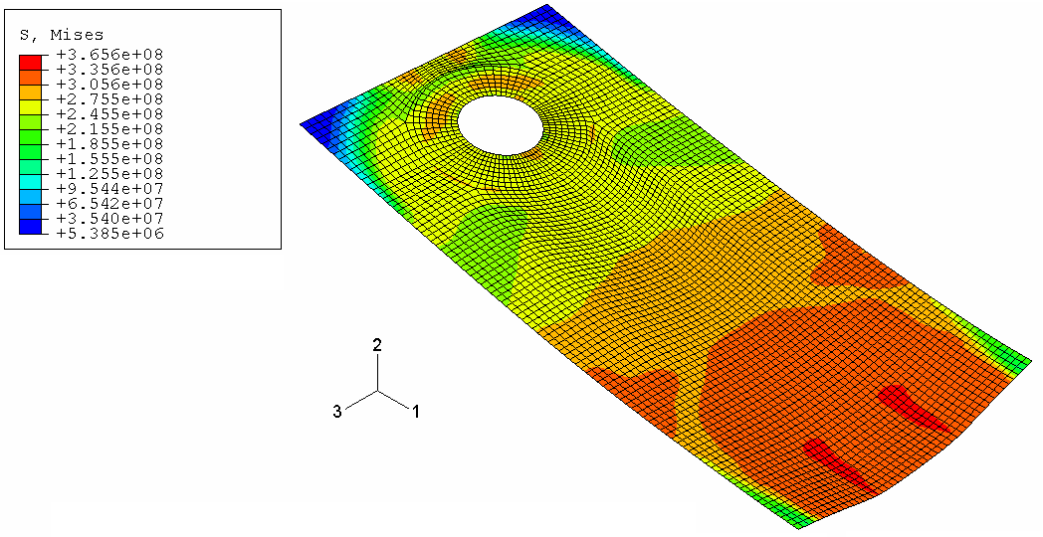

Figure 6.27. Maximum deformation of Simplified model 7 at 0.0011025 s

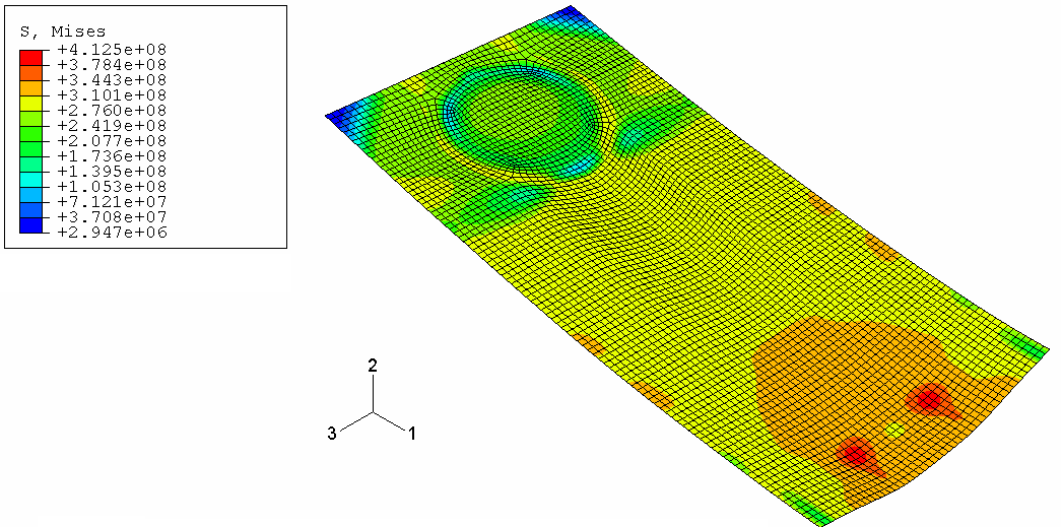

Figure 6.28. Maximum deformation of Simplified model 8 at 0.0011025 s

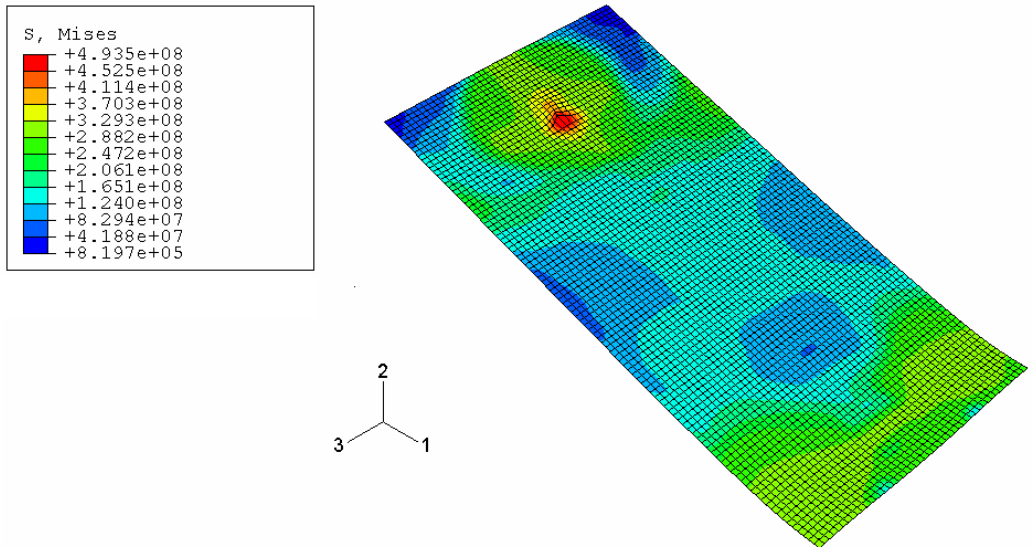

Figure 6.29. Maximum deformation of Simplified model 9 at 0.00162 s

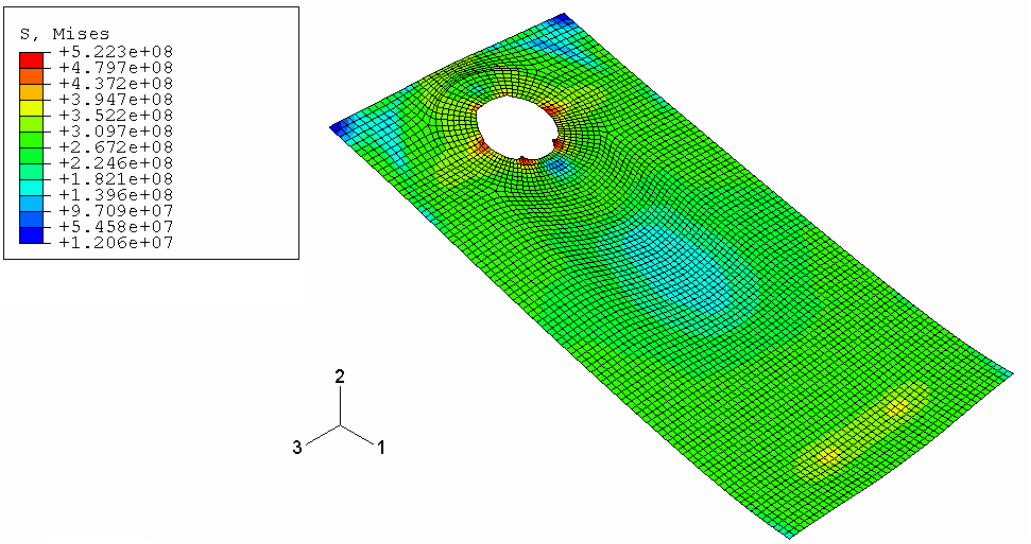

Figure 6.30. Maximum deformation of Simplified model 10 at 0.001215 s

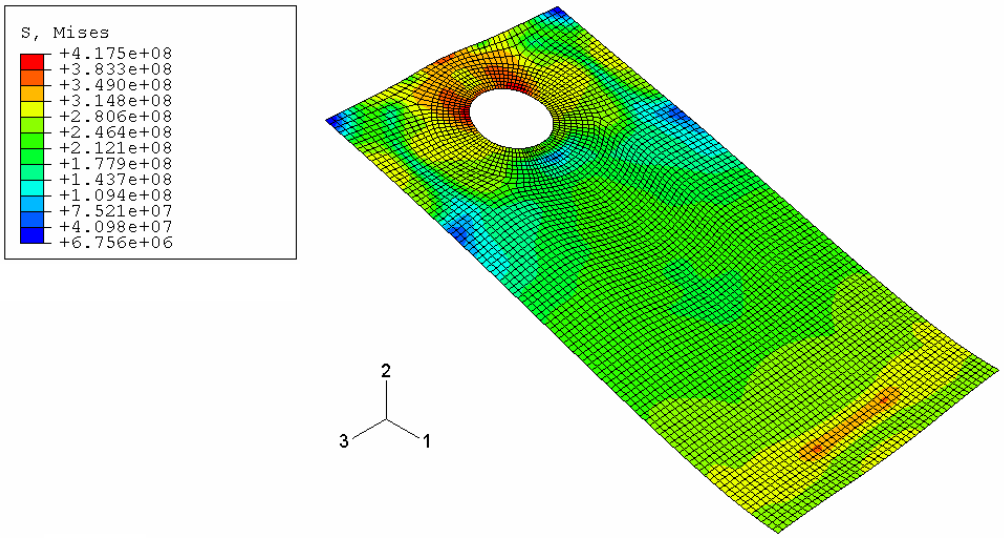

Figure 6.31.Maximum deformation of Simplified model 11 at 0.00132 s

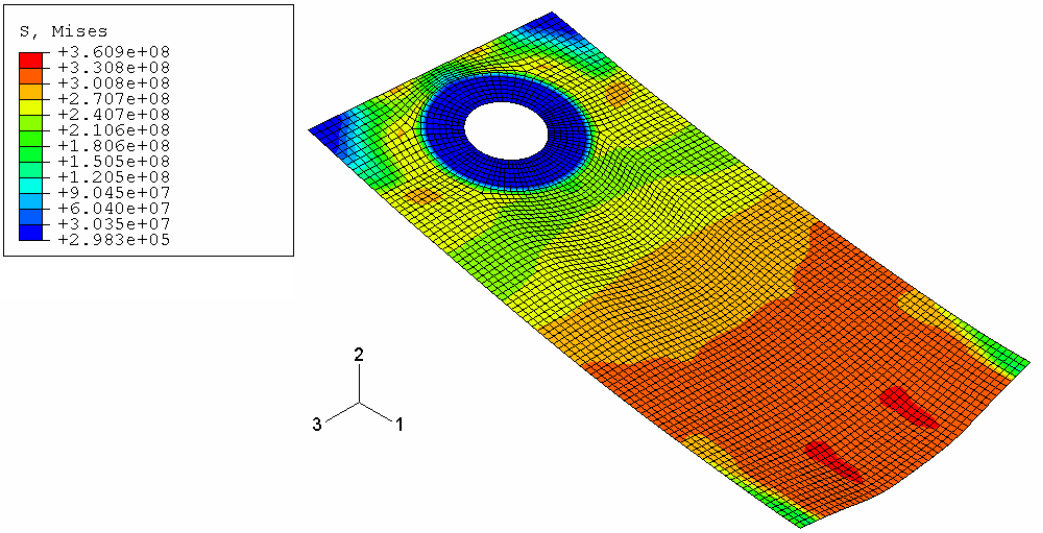

Figure 6.32. Maximum deformation of Simplified model 12 at 0.0011025 s

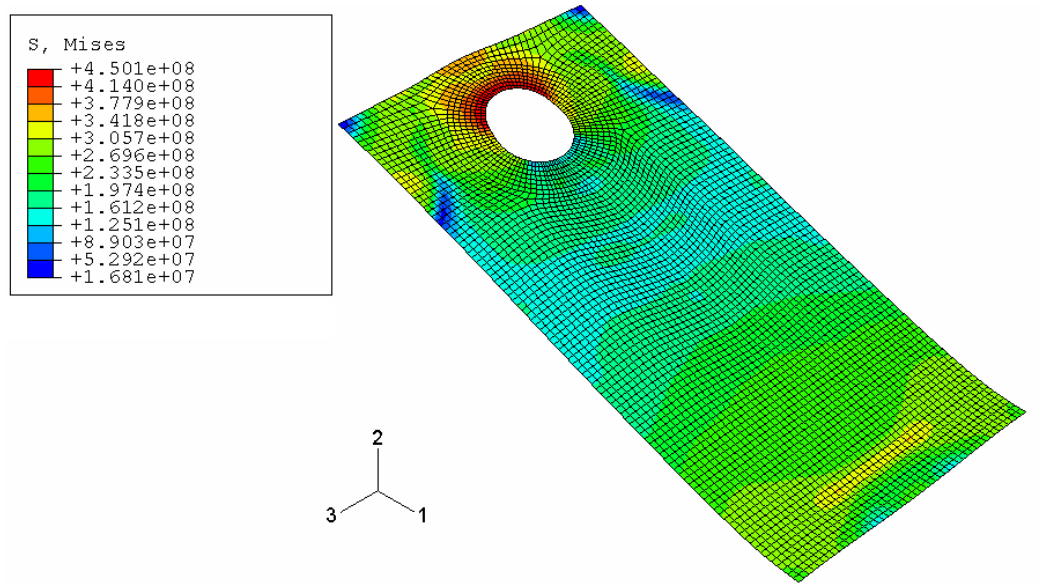

Figure 6.33. Maximum deformation of Simplified model 13 at 0.00157 s

According to the results of the analyses, at higher impact loads (configuration 2), the simplified bolt models 1, 5, 6, 9, and 10 overestimate the plastic strain on the perimeter of the bolt holes. They predict the plastic strains at least two times larger than the full model's. The simplified models 3, 4, 7, 8, and 12 underestimate the plastic strain of the perimeter, while they highly over estimate at the middle of the plate. Because the total kinetic energy transferred to the structure is the same for each case and it is largely transformed into strain energy of deformation, it is understandable that if a model highly overestimate the deformation at one location it is likely that it underestimates at other locations. As for the modeling complexity concerns, these models are quite easy, they have

limited number of elements and they need less contact relations than the full model. These models predict the plastic strain approximately 40-50 percent less than the full model at the perimeter of the bolt hole. Simple stated, they perform stably over the courses of the analyses. For small loads, some models predict the plastic strain around the bolt holes well; but they fail for high loads.

Tables 6.1-7 indicate that simplified model 1 predicts the strain values around the bolt hole in a stable fashion. However, for modeling burden concerns, making this model is more complicated in comparison to other simplified models.

In the simplified model 10, always twelve connector beam elements were used. If the mesh density of the sheets is increased the number of connector elements should be increased due to localization effect. However, when highly dense mesh is used, then there should be so many connector elements in the model, which makes this model impracticable. The model used here has constant number of elements through the analyses with various mesh densities. For this reason, the plastic strain values increase with the increased mesh density due to localization effect.

6. CONCLUSION

This research involved development of finite element models of bolted joints subject to impact loading. In order to accurately determine the response of the structure, a detailed model was developed that accounted for almost all of the factors that had influence on the stress and strain states in the joined sheets. In order to obtain the structural response with a minimal computational burden, a number of simplified models were developed. The full model was used as a benchmark for the accuracy of the simplified models.

All of the simplified models saved computational time accept simplified model 1 when compared with the full model using the same mesh density. The saving in computational time savings is about %80-90. Because the sheets are discretized with solid elements in the full model, many elements should be used through the thickness to obtain convergence unlike the simplified models, in which shell elements are used. For this reason, convergence of the simplified models can be obtained with coarser meshes. In view of that, actual savings in time are much larger in practice.

Simplified model 1 generally overestimates the plastic strain around the bolt hole and also its computational burden is high.

Simplified models 5 and 6 give acceptable results with coarse meshes. However, they give much higher strain values when the mesh is fine.

Simplified models 9 and 10 highly overestimate the plastic strains near the bolt hole. Besides, their artificial energies stored in elements are beyond the acceptable limits. Therefore, these models are not recommended, especially under high loads.

Simplified models 2-4 and 7-8 and 12 give better results when the loads are low. Even though, they underestimate the strain values under high loads, they yield consistent results with different mesh densities.

Simplified model 13 overestimates plastic strains around the bolt hole by about three times.

Among the simplified models, simplified model 11 most accurately predicts the physical behavior of the structure for different loading cases and mesh densities.

In pre-stressed bolted joints, due to decreasing effect the plastic strain values around the bolt, the simplified models' predictions generally shows better performances.

Therefore, in view of effectiveness and usefulness and modeling concerns, simplified model 11 is recommended.

APPENDIX A: DETAILED LITERATURE SURVEY

A number of studies were conducted to develop simplified models for bolted joints using finite elements. Mistakidis, and Baniotopoulos s [1] aimed to simulate steel bolted connections by introducing an effective two-dimensional geometrical simplification to the respective three-dimensional one. The thickness of the plane stress elements was properly adjusted in order to take into account the three-dimensional properties of the structure. A certain value was assigned to the thickness of the T-stub except of the region of the holes. For the nut, the shank, the washer and the region of the hole of the T-stub, the thickness of the corresponding finite elements was assigned according to Figure A.1. The interaction between these three bodies was taken into account by considering unilateral contact conditions between them. The joint was subjected to static loading. Pre-tensioning of the bolts was not considered in the work.

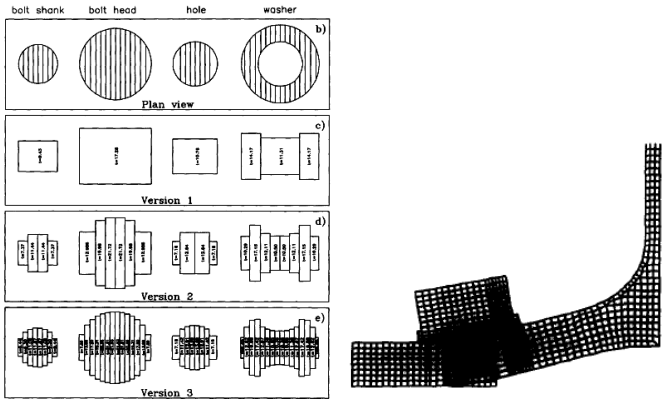

Figure A.1. Thickness values for the different versions of the F.E. mesh and the deformed shape of the structure for various load increments [1]

Bursi and Jaspart [2,3,4], carried out some simulations to verify an assemblage of beam elements of bolt model. In the 3-D modeling**,** brick elements, brick elements with reduced integration and brick elements with incompatible modes were used. The contact element which allows the finite sliding interaction was considered for these applications. In the simplified modeling, beam elements were employed for modeling the bolt. The beam sections adopted to reproduce the bolt head were calibrated with finite element analyses by subjecting the 3-D bolt head to combined bending and shear. Beam sections were also

computed analytically on the basis of the actual bolt head geometry. In particular, the inner beams were assumed to have flexural and shear stiffnesses four times larger than the relative stiffnesses of the outer beams. The bolt was reproduced through the simplified model suggested by adopting 16 beams for the inner part and the same number of beams for the outer part of the bolt head. However, only five elements were adopted to discretize the bolt shank. In addition, the bolt head beam assemblage was connected to the solid assemblage through hinges at the beam ends.

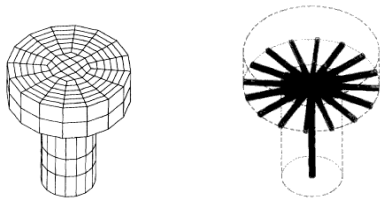

Figure A.2. 3D continuum model and spin model [3, 4]

Static loading was applied to the joint. Preloading forces were applied as initial stresses in the bolts. In conclusion, C3D8I elements behave particularly well in the inelastic range, being purposely designed for bending dominated problems. As expected, C3D8R elements underestimate the plastic failure load, whereas the prediction with C3D8 elements appears to be unsatisfactory owing to the overestimation of the plastic failure load [2,3,4].

Chung and Ip [5,6] tried three-dimensional solid elements with non-linear material, geometrical and contact analysis to investigate the structural performance of bolted connections under static shear loading. Three-dimensional eight-node iso-parametric solid elements were used to model all the components. Contact interfaces between strips and the bolt, the washer and steel plates were modeled by contact elements. The bolt was assumed to be threadless and formed an integral component with the washer. The bolt–washer component was assumed to be linear elastic throughout the analysis. Furthermore, the root of the bolt–washer component was fixed in space by constraining the associated nodes. For ease of meshing, an artificial small hole of 1 mm diameter was provided through the centre-line of the bolt–washer component. Furthermore, the finite element mesh was refined locally in the vicinity of the bolt hole. The aspect ratios of those elements near the bolt hole were kept small to reduce the shear locking effect in the elements.

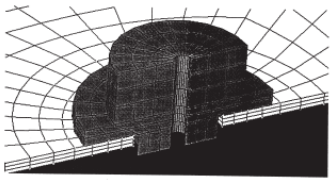

Figure A.3.Finite element mesh for the connection [5]

The joint was subjected to static loading. Bolt clamping was also incorporated by considering a bolt shank whose length was less than the thickness of the cold-formed steel strip typically by 5%, and thus, initially the washer penetrates into the cold-formed steel strips in the geometry of the finite element model. During the first iteration of the analysis, the washer and the cold-formed steel strips would push against each other by inducing tensile stresses in the bolt shank while compressive stresses in areas beneath the washer were established [5,6].

At the study of Kishi *et al*. [7], all components of the connection were modeled using eight-node linear brick elements. It was chosen because a C3D8 element with full integration is precise in the constitutive law integration and is suitable for plasticity problems. Shapes of bolt shank, head, and nut were precisely taken into account in modeling. Small sliding contact pair definition was employed. The model was analyzed using three loading steps. In the first step, pretension force was applied. In the second step, the prescribed bolt load was replaced by changing the length of pretension section back to the initial length. Bolt pretension equaled to 70 percent of tensile strength of bolt. Loading was applied statically [7].

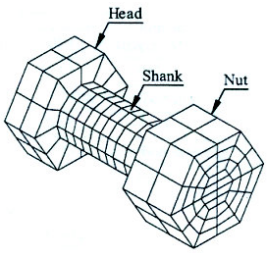

Figure A.4. Mesh pattern of bolt model [7]

A finite element investigation of the behavior of T-stub flanges were presented and compared with experimental data by Swanson, Kokan, and Leon[8]. A three dimensional T-stub model were constructed with brick and wedge elements. The monolithic sections representing the column flange and beam flange were made up of C3D8, 8 node brick elements. The sections were modeled as rigid by giving them a linear elastic material response with a modulus of elasticity 10 times that of steel. The bolts were made up of an inner core of C3D15, 15 node wedge elements with outer layers of C3D20, 20 node brick elements. The shanks of the bolts were modeled as prismatic. The heads of the bolts were modeled as cylinders, having a constant thickness approximately equal to the average thickness of the actual bolt head. Bolts are subjected to full restraint of the free ends of the bolt shanks. The ABAQUS solver encountered convergence problems stemming from perceived rigid body motion. To overcome this, the nodes along the edges of the T-stub flange that were in initial contact with the column flange were restrained for the duration of the bolt pre-tensioning load step. The bolts were pre-tensioned by applying support displacements to the restrained ends of the bolt shanks. The prescribed bolt displacements were calculated assuming that the bolts remained elastic with a target pretension

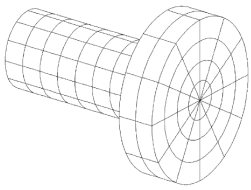

Figure A.5. 3D solid bolt model [8]

In another study [9], the connecting bolts were assumed to be rigid. Finite element analysis was carried out using eight node incompatible hexahedral elements. The contact areas were the bolt shank-to-bolt holes and bolt head-to-components. Pretension was assigned via ABAQUS bolt loads feature. Static tension loading was applied to the bolted joint [9].

Sabuwala *et al* [10] analyzed the behavior of the selected connection elements under blast loads and benchmarked the performance of the models. Due to small time durations and high pressure loads required for the study, the finite element models were created using 8-noded continuum (brick) elements with reduced integration. Wedge elements

(C3D6) were used to model curved regions of the beam. Elasto-plastic material properties with isotropic hardening were selected to simulate material behavior of all components in the finite element model except the welds. A tied contact formulation was used for the welds and small-sliding formulation was used for the other interacting parts such as bolts–bolt holes, bolt–tabs, tabs–beam, and cover plates–beam. This first response cycle was minimally affected by damping in the system and damping effects were subsequently neglected in the theoretical procedure. Thus, damping was not taken into the account. The bolt and the nut are considered as different parts. The hexagonal bolt heads were modeled as cylinders.

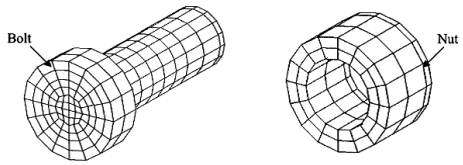

Figure A.6. Finite element models of the bolt and the nut [17]

The effect of several geometrical and material parameters on the overall moment–rotation response of two connection configurations subject to static loading was studied by Citipitioglu and Haj-Ali [11]. The bolt-nut assembly was considered as a monolithic structure. The nut, namely, were not modeled as an independent part. The hex bolt heads are modeled as cylinders, taking into account the effect of the washers by averaging the diameters. The bolt holes were taken as slightly larger than the bolt shaft diameter. The geometric model was discretized using C3D8I eight-node brick elements with full integration and incompatible modes. The performance of this continuum element was compared with other formulations and it was shown to give better results for bending-dominated problems with relatively small thickness. C3D6 six-node wedge elements were also used to model the core of the bolts. Contact between all parts was explicitly modeled. The contact areas were the bolt shank-to-bolt holes and bolt head-to-components. The washers were not modeled. Under static loading conditions, the bolted joint was examined. The pretension in the model was achieved in two steps. In the first step, the length of the bolt was chosen shorter than the total thickness of the connecting plates. In the second step, the contact between the displaced bolt head and its respective surface was activated and the imposed displacement was released. In order to determine the displacement needed to induce the desired pretension value in the bolts, a method was proposed. In this method,

models of a plate with a single headed bolt were separately created to determine the bolt force–displacement relation with different plate thicknesses [10].

Ju *et al* [12] performed 3D elasto-plastic finite element simulations to study the bolted connection behavior. The bolt clearance, the bolt head, the washer, the deformable bolt and the friction were included in order to simulate the actual structural behavior of the bolted connection. Eight-node 3D isoparametric elements with the incompatible mode, 3D node-to-surface contact elements and node-to-Hermit-surface contact elements were used in the finite element mesh. To avoid the bolt rotation, the side and center nodes on the bottom of the bolt were fixed in appropriate direction. Static loading was applied to the joint. Bolt pre-tension was induced by using initial displacement scheme

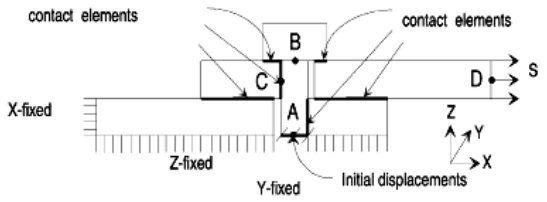

Figure A.7. Boundary conditions and contact surfaces [11]

Yorgun *et al* [13] used brick elements with eight nodes in three-dimensional modeling of plate sections. Bolts were modeled with tetrahedron elements which capable of meshing irregular shapes. Contact surfaces were meshed with contact element and target segment elements. The contact and bearing interactions between the bolt shanks and bolt holes were neglected. Static loading was applied to the joint. Equivalent initial strain approach was adopted for the pretension in the bolt shank [12].

Three kinds of finite element models were proposed by Reid and Hiser [18] for bolted joints. The discreet based clamping, DBC, model utilized a discrete spring element to preload the bolt and generate the clamping force between the slip base plates which were modeled with deformable fully integrated solid elements. The bolts, nuts, and washers, on the other hand, were modeled after the actual component geometry with rigid solid elements. Clamping forces were applied using a single centrally located discrete spring element. The spring was defined to act along the axis of the rigid bolt shaft, connecting the head of the bolt to the center of the nut. Secondly, a translational joint was

placed between the nut and bolt shaft in order to constrain the nut to movement only along the bolt shaft. To produce a desired preload, the spring was given an initial offset, which induced an initial force in the spring.

The stress based clamping, SBC, bolt model that utilized deformable solid elements with the material properties of steel, which when stretched through an initial deflection, would produce the desired preload in a way consistent with an actual bolt tightening. The SBC model incorporated the bolt head, bolt shaft, and nut as an integrally meshed solid body. The washers remain rigid. The preload is achieved by pre-stressing the elements. This was accomplished by assigning values for the stress tensor at each integration point within each solid element. A Fortran program was used to apply the pre-stress along the bolts' longitudinal axis to every integration point of every solid element in the bolt shaft. The SBC model was modified by using a deformable material model for washers instead of rigid material models. This modified model was referred to as the stress-based clamping with deformable washers model (SBC-DW) as seen Figure 1.8. All other features of the model were identical to SBC.

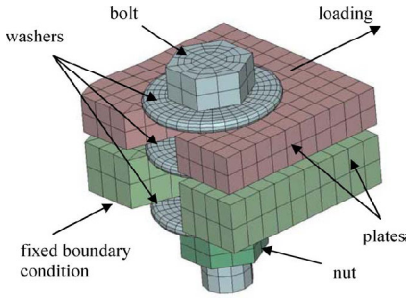

Figure A.8.Joint model [18]

An analytical torque-preload relation was used to predict accurately bolt pretension. Dynamic loading was applied to the bolted joint. Higher accuracy was achieved when a deformable washer was added to the SBC model. Although exceptional force-displacement correlation was attained with the SBC-DW model, its' use may be unwarranted in some circumstances due to increased computational cost [18].

Butterworth [15] conducted materially non-linear three dimensional finite element analyses. Three dimensional solid hexahedral elements comprising 8 nodes each were used

to model the beam flanges, end plate and connecting column flange. The bolts were modeled using beam elements, having 2 nodes each with 3 degrees of freedom, for the bolt shank and brick elements for the head and nut as shown in Figure 14. The bolt holes were modeled as square cut-outs in the end plate and column flange. The bolted joint was examined under the condition of static loading. Bolt pretension was included in the model as an initial pre-stress in the BRS2 elements

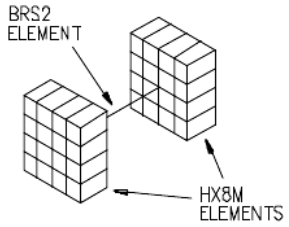

Figure A.9.Finite element model of the bolt [13]

The McCarthy *et al* [16] developed three-dimensional finite element models to study the effects of bolt–hole clearance on the mechanical behavior of bolted composite joints. Both linear 8-noded and quadratic 20-noded iso-parametric hexahedral elements were used for comparison. Wedge elements were used to form the core of the bolt. To avoid potential rigid body modes, light springs were attached to the components not fully constrained such as the bolt, washers and bottom laminate. Static loading was applied by means of prescribed displacement. To simulate bolt pre-load due to applied torque, coefficients of thermal expansion were given to one of the washers. This washer was then subjected to a positive temperature differential prior to mechanical loading which had the effect of stretching the bolt and clamping the laminates.

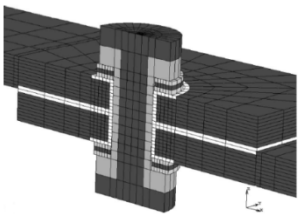

Figure A.10.Contact bodies defined by possible contacting elements only: Section through single-bolt model highlighting contact bodies [14]

The dynamic frictional contact analysis of a bolted joint under harmonic loading was investigated by Oldfield *et al*. 17]. Both solid blocks were composed of eight-noded, linear, reduced-integration elements. The bolt–nut component was constructed from six-noded, linear, wedge elements making up the shaft and eight-noded, linear, reduced-integration elements in the bolt head and nut, as shown in the Figure 1.11. The washers were not included in the model. The external diameters of the bolt head and the nut in the finite element model were taken to the same as those of real bolt and nut. The contact relation between the bolt hole and bolt shaft was not considered in the model. The bolted joints were subjected to cycling loading. To reduce the computational time, the contact analysis for the joint under the initial preload was conducted in ABAQUS/Standard. This produced accurate results that were then exported into ABAQUS/Explicit. A detailed finite element model of a bolted joint was also created to provide the necessary information about the response of the joint to a dynamically applied torque

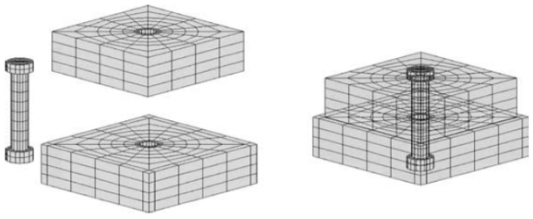

Figure A.11.The finite element models of the three components and assembled configurations [19]

Kwon *et al*. [18] performed the 3D finite element simulation and developed practical simplified models to study the bolted connection behavior. In the 3-D finite element modeling of the work**,** an incompatible 8-node solid elements and contact elements were used as can be seen the first from the left in Figure 1.12. In the hybrid modeling, unlike the 3-D model, the elements for the bolt head and the nut were changed to shell elements, whereas the shank of the bolt was again modeled with solid elements, the second in the figure. In the simplified shell element modeling**,** shell elements were used for the bolt shank with a cylindrical shape. The diameter of the cylindrical shell component was equal to that of the bolt shank. In the 2-D Shell-beam element modeling, unlike the shell element model, the bolt shank was modeled by using an equivalent beam element.

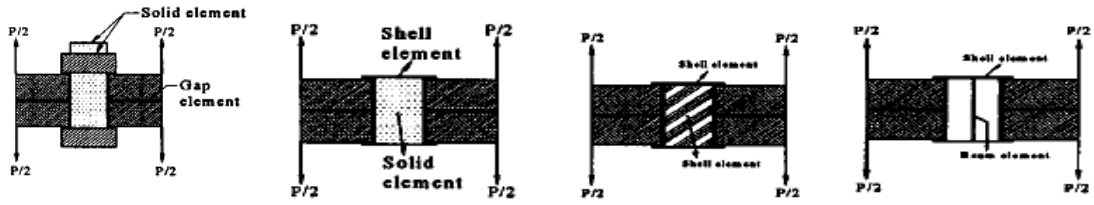

Figure A.12. Finite element models for bolted joints loaded in tension by forces [15]

The external load was axi-symmetrically distributed. The reseearchers used slightly different models for dynamic analysis from that of static analysis. Besides, they used shell elements to model bolts. A few modifications were made to adopt the static practical models to the dynamic analysis. Two members were united at a contact part, where the bonding forces resulting from the preload were united via diagonal lines. By the other contact parts were divided with the absence of contact elements. The practical model was simplified based on the assumption that a gap element could not be applied to a dynamic analysis. As expected, the detailed model is the most accurate model among the others. However, shell-beam model had an unacceptable error. The results of the hybrid and shell models were almost identical to that of the 3-D model, confirming that the two practical models were effective

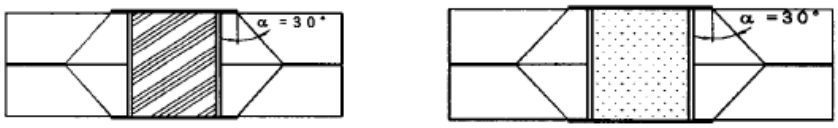

Figure A.13. Practical models for dynamic analysis [15]

Kim *et al*. [19] introduced four different of finite element models in order to investigate a structure with bolted joints. All the proposed models took into account pretension effect and contact behavior between flanges to be joined. In the 3-D modeling of that study**,** the bolt-nut assembly was considered as monolithic. The solid bolt model was meshed by using three-dimensional eight-node brick elements. In addition, surface-to-surface contact elements were used on the interfaces between the bolt head and the upper plate, the nut and the lower flange, and between the upper and lower flanges. In the bolt model, in order to apply clamping force, virtual thermal deformation method was employed. In this method, the thermal expansion coefficient was assumed to be unit and

the temperature difference ΔT is calculated by the following equation: $\Delta T = \frac{4.P_0}{\pi.d^2 E}$ where E was elastic modulus of the material, d was an effective diameter of the bolt, and P_0 was the clamping force.

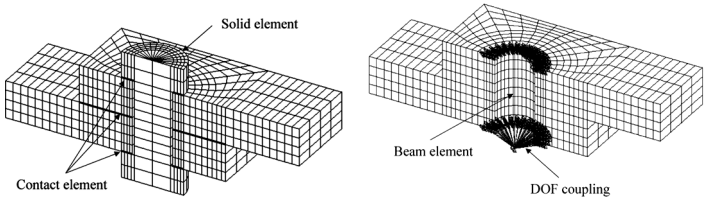

Figure A.14. Solid bolt model and coupled bolt model [16]

Three simplified model were proposed in that study: Coupled bolt model*:* In the coupled bolt model as shown in Figure 1.14., the stud of the bolt was modeled by a beam element, and the nodes corresponding to the bolt head and the nut were connected to the stud by means of the DOF coupling. The beam element was a uniaxial element with tension, compression, torsion, and bending capabilities. In this approach, since only a single beam element was used to represent the bolted joint, the number of finite elements was significantly reduced compared to the solid bolt model. The pretension effect was considered by directly applying an initial strain ε_0 to the stud as given by: $\varepsilon_0 = \frac{4.P_0}{\pi.d^2 E}$ However, there was no need to introduce contact elements between the bolt and the plates in this bolt model.

Spider bolt model [19]*:* The spider bolt model was composed of three-dimensional beam elements for all components of the bolt, i.e. stud, head and nut as shown in Figure 1.15. The stud was represented by a single beam element as in the coupled bolt model, and both the head and the nut were also modeled with a series of beam elements in a web-like fashion. Since the head (or nut) and flange were connected to each other by a beam element, various loads can be transferred and the head (or nut) stiffness can be accounted. However, in the spider bolt model, physical properties of the beam elements such as the cross-sectional area, the area moment of inertia, the height had to be selected appropriately to correctly reflect the stiffness of the bolted joints. To do this, the total volume of beam elements for the head (or nut) was assumed to be equal to that of the actual head (or nut) in this study.

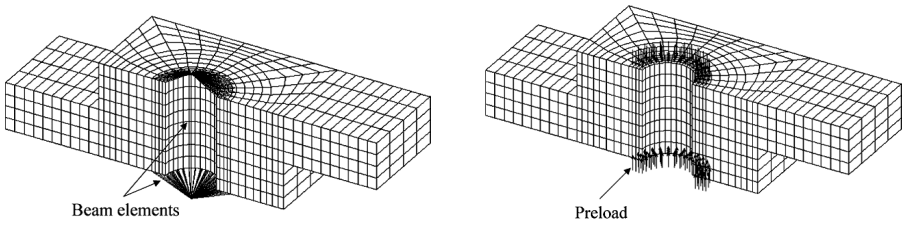

Figure A.15. Spider model and no-bolt model [16]

No-bolt model[19]*:* In this model, there were no finite elements to directly represent the bolt components as shown in Figure 1.15.b. The pressure corresponding to the clamping force was imposed on the washer surface to simulate the pretension effect. The no-bolt model cannot consider the influence of the bolt stiffness, and change in the bolt load, due to application of a clamping force, were not accounted for. It was noticed that this no-bolt model should be used in case it is not required to consider the bolt stiffness and no separation takes place between parts.

Static and dynamic loading were applied to the bolted joints. The solid bolt model, which was modeled by using three-dimensional brick elements and surface-to-surface contact elements between the head/nut and the flange interfaces, provided the most accurate responses compared with the experimental results. In view of effectiveness and usefulness, the coupled bolt model was also recommended. [16]

In the study of Razavia *et al*. [20], the effect of pre-stress force in the bolt was incorporated by adding load vector to the total load vector at the normal DOF of the bolt ends. A half cycle of loading–unloading was applied to the bolted joint. In the simplified modeling**,** to model axial effects of the bolt shank, a truss element with one axial degree-of-freedom (DOF) at each end was used. It was also assumed that bolt head and nut act as rigid plates in contact with connecting surfaces at all times and unable to undergo bending. This meant that all the nodes in contact with bolt head (or bolt nut) move together in the axial direction and they were assigned the same normal DOF in the axial bolt shank direction (Figure 1.16).

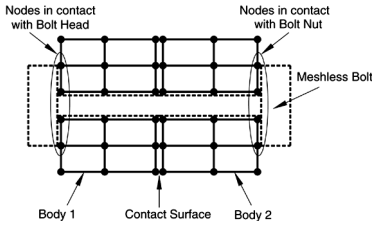

Figure A.16.Invisible bolt connecting to bodies [24]

The plates were discretized with 8-noded solid elements. The nodes in contact with bolt head (or nut) were restricted to move in the radial direction of bolt and their movements were dependent on the bolt's elongation and end rotations [24].

A finite element procedure was implemented to analyze a two-step loaded structure system in terms of ABAQUS/Standard and ABAQUS/Explicit tools by Ren and Wang [21]. In this model, the boundary conditions were prescribed such that the degrees of freedom of the nodes on symmetric surfaces whose directions were perpendicular to the corresponding symmetric surfaces were restrained. The analysis of the pre-stressing step was conducted by using ABAQUS/Standard tool. The joint was also analyzed under impact loading. In order to model the preloaded screw, two steps were employed: (1) Preload of the system by the pre-tension of screws; (2) Release of external forces and constraints from the system. By the combination of ABAQUS/Standard tool and ABAQUS/Explicit tool, a non-linear finite element simulation procedure was established for the pre-stressed structure under impact loading condition [25].

In the study of Hendricks and Wekezer [20], two different simplified finite element models were investigated to study the bolted connection of guardrails. Firstly, they merged the nodes between the separate parts. Besides, they obtained the same effect of that by using nodal constraints in order to fix translational degrees of freedom between the connected nodes. Secondly, tied node sets with failure were used without requiring a material model with a failure criterion. Lastly, elastic-plastic springs were used. An initial elastic spring constant, a yield force, and a plastic spring constant were introduced. Throughout this study, kinematic-isotropic material model was used. The joint was analyzed under impact loading.

In the work of O'Daniel *et al*. [21], two different models were used in order to adopt the bolted joints. The first one numerically welded adjacent nodes of plates that were held

together by bolt in actual joint. The second modeled the bolts by means of connecting beam elements through the mesh of the panels. The cross sectional areas, lengths were as they actually were. The panels were modeled by eight-noded tetrahedral continuum elements. Friction was neglected due to its negligible effects during the transverse impact phenomena.

APPENDIX B: SOME SELECTED RESULTS

Table B.1.Analysis times of the models for configuration 1

Model Name configuration 1	Mesh Size	Analysis Time (s)	Analysis Time Normalized
Full Model	0.0005	59980	336.4
	0.00066	17831	100.0
	0.001	2503	14,0
	0.002	284	1.6
Simplified Model-1: Full Model with Shell	0.0005	58863	330.1
	0.00066	40753	228.6
	0.001	7132	40.0
	0.002	697	3.9
Simplified Model 2: Rigid Shank with Coupling	0.0005		
	0.00066	2676	15.0
	0.001	693	3.9
	0.002	183	1.0
Simplified Model 3: Coupling Constraint with Hole	0.0005		
	0.00066	2210	12.4
	0.001	825	4,6
	0.002	79	0.4
Simplified Model 4: Coupling Constraint without Hole	0.0005		
	0.00066	5931	33.3
	0.001	1610	9.0
	0.002	226	1.3
Simplified Model 5: Vertical Connector Beams	0.0005	4489	25.2
	0.00066	1893	10.6
	0.001	789	4,4
	0.002	72	0.4
Simplified Model 6: Vertical Connector Beams On Washer Outer Line	0.0005		
	0.00066	1694	9.5
	0.001	608	3.4
	0.002	161	0.9
Simplified Model 7: Tie Constraint with Hole	0.0005		
	0.00066	2497	14,0
	0.001	831	4,7
	0.002		

Table B.1.Analysis times of the models for configuration 1 (continue)

Simplified Model 8: Tie constraint without hole	0.0005		
	0.00066	3197	9.5
	0.001	938	3.4
	0.002	80	0.9
Simplified Model 9: Connector One Beam	0.0005	3101	17,4
	0.00066	1366	7.7
	0.001	618	3.5
	0.002	233	1.3
Simplified Model 10: Cross Connector Beam	0.0005		
	0.00066	2195	12.3
	0.001	1437	4,7
	0.002		1.4
Simplified Model 11:Rigid Shell Bolt	0.0005	5534	31.0
	0.00066	2542	14,3
	0.001	707	4,0
	0.002	205	1.1
Simplified Model 12: Cross Coupling Constraint	0.0005	4479	25.1
	0.00066	2047	11.5
	0.001	584	3.3
	0.002	181	1.0

Table B.2. Maximum plastic strain values of the models for configuration 1

Model Name configuration 1	Mesh Size	Max. Plastic Strain	Normalized
Full Model	0.0005	0.00659742	103.1
	0.00066	0.0063988	100.0
	0.001	0.00413283	64,6
	0.002	0.0	0.0
Simplified Model 1: Full Model with Shell	0.0005	0.0146977	229.7
	0.00066	0.0136301	213.0
	0.001	0.0111919	174,9
	0.002	0.00782744	122.3
Simplified Model 2: Rigid Shank with Coupling	0.0005		
	0.00066	0.00115306	30.1
	0.001	0.00104534	28.5
	0.002	0.000736346	22.0

Table B.2. Maximum plastic strain values of the models for configuration 1 (continue)

Simplified Model 3: Coupling Constraint with Hole	0.0005		
	0.00066	0.00204523	32.0
	0.001	0.00188093	29.4
	0.002	0.00174927	27.3
Simplified Model 4: Coupling Constraint without Hole	0.0005		
	0.00066	0.00214785	33.6
	0.001	0.00266216	41.6
	0.002	0.00118683	18.5
Simplified Model 5: Vertical Connector Beams	0.0005	0.00266387	41.6
	0.00066	0.00207199	32.4
	0.001	0.00163722	25.6
	0.002	0.00172046	26.9
Simplified Model 6: Vertical Connector Beams On Washer Outer Line	0.0005		
	0.00066	0.00281992	44,1
	0.001	0.00264694	41.4
	0.002	0.00252617	39.5
Simplified Model 7: Tie Constraint with Hole	0.0005		
	0.00066	0.00351725	55.0
	0.001	0.00305397	47.7
	0.002		
Simplified Model 8: Tie constraint without hole	0.0005		
	0.00066	0.00292455	45.7
	0.001	0.00274981	43.0
	0.002	0.00225799	35.3
Simplified Model 9: Connector One Beam	0.0005	0.00865863	135.3
	0.00066	0.00634318	99.1
	0.001	0.00532768	83.3
	0.002	0.00209162	32.7
Simplified Model 10: Cross Connector Beam	0.0005		
	0.00066	0.00308931	48.3
	0.001	0.00214785	33.6
	0.002	0.00185199	28.9
Simplified Model 11:Rigid Shell Bolt	0.0005	0.00464218	173.7
	0.00066	0.000573066	117.2
	0.001	0.0000950889	65.3
	0.002	0.00000218	95.0

Table B.2. Maximum plastic strain values of the models for configuration 1 (continue)

Simplified Model 12: Cross Coupling Constraint	0.0005	0.000697975	110.6
	0.00066	0.000586022	110.0
	0.001	0.00044942	88.0
	0.002	0.000302184	73.4

Table B.3.Maximum von Mises stress values on middle zone of the models for configuration 1

Model Name configuration 1	Mesh Size	Max. von Mises At the Middle (MPa)	Normalized
Full Model	0.0005	351	100.9
	0.00066	348	100.0
	0.001	33.1	9.5
	0.002	37.0	10.6
Simplified Model 1: Full Model with Shell	0.0005	368	105.7
	0.00066	372	106.9
	0.001	361	103.7
	0.002	355	102.0
Simplified Model 2: Rigid Shank with Coupling	0.0005		
	0.00066	357	102.5
	0.001	339	97.5
	0.002	343	98.7
Simplified Model 3: Coupling Constraint with Hole	0.0005		
	0.00066	349	100.4
	0.001	351	100.9
	0.002	341	98.0
Simplified Model 4: Coupling Constraint without Hole	0.0005		
	0.00066	351	100.9
	0.001	337	96.7
	0.002	346	99.3
Simplified Model 5: Vertical Connector Beams	0.0005	359	103.0
	0.00066	347	99.9
	0.001	362	104,1
	0.002	355	101.9

Table B.3.Maximum von Mises stress values on middle zone of the models for configuration 1 (continue)

Simplified Model 6: Vertical Connector Beams On Washer Outer Line	0.0005		
	0.00066	355	102.1
	0.001	355	102.1
	0.002	356	102.2
Simplified Model 7: Tie Constraint with Hole	0.0005		
	0.00066	358	102.8
	0.001	358	102.9
	0.002		
Simplified Model 8: Tie constraint without hole	0.0005		
	0.00066	356	102.4
	0.001	350	100.5
	0.002	349	100.4
Simplified Model 9: Connector One Beam	0.0005	388	111.6
	0.00066	388	111.6
	0.001	373	107.1
	0.002	348	99.9
Simplified Model 10: Cross Connector Beam	0.0005		
	0.00066	340	97.7
	0.001	351	100.9
	0.002	351	100.8
Simplified Model 11:Rigid Shell Bolt	0.0005	382	109.7
	0.00066	351	100.9
	0.001	354	101.7
	0.002	354	101.6
Simplified Model 12: Cross Coupling Constraint	0.0005	376	108.1
	0.00066	368	105.9
	0.001	370	106.2
	0.002	367	105.5

Table B.4. Center displacement values of the models for configuration 1

Model Name Configuration 1	Mesh Size	Center Displacement (m)	Center Displacement Normalized
Full Model	0.0005	-0.00376915	98.8
	0.00066	-0.00381385	100.0
	0.001	-0.00385152	101.0
	0.002	-0.00710257	186.2
Simplified Model 1: Full Model with Shell	0.0005	-0.00364435	95.6
	0.00066	-0.00362627	95.1
	0.001	-0.00363119	95.2
	0.002	-0.00359915	94,4
Simplified Model 2: Rigid Shank with Coupling	0.0005		
	0.00066	-0.00324486	85.1
	0.001	-0.00328875	86.2
	0.002	-0.00334703	87.8
Simplified Model 3: Coupling Constraint with Hole	0.0005		
	0.00066	-0.00338671	88.8
	0.001	-0.00338796	88.8
	0.002	-0.00339656	89.1
Simplified Model 4: Coupling Constraint without Hole	0.0005		
	0.00066	-0.00352139	92.3
	0.001	-0.00339975	89.1
	0.002	-0.00339837	89.1
Simplified Model 5: Vertical Connector Beams	0.0005	-0.00358177	93.9
	0.00066	-0.00351556	92.2
	0.001	-0.00344698	90.4
	0.002	-0.00340365	89.2
Simplified Model 6: Vertical Connector Beams On Washer Outer Line	0.0005		
	0.00066	-0.00330933	86.8
	0.001	-0.00329751	86.5
	0.002	-0.00329343	86.4
Simplified Model 7: Tie Constraint with Hole	0.0005		
	0.00066	-0.00320641	84,1
	0.001	-0.00320155	83.9
	0.002		
Simplified Model 8: Tie constraint without hole	0.0005		
	0.00066	-0.00327508	85.9
	0.001	-0.00327287	85.8
	0.002	-0.00327649	85.9

Table B.4. Center displacement values of the models for configuration 1 (continue)

Simplified Model 9: Connector One Beam	0.0005	-0.00401102	105.2
	0.00066	-0.00393806	103.3
	0.001	-0.00382664	100.3
	0.002	-0.0036093	94,6
Simplified Model 10: Cross Connector Beam	0.0005		
	0.00066	-0.00361083	94,7
	0.001	-0.00352139	92.3
	0.002	-0.00343079	90.0
Simplified Model 11:Rigid Shell Bolt	0.0005	-0.00272667	71.5
	0.00066	-0.00292772	76.8
	0.001	-0.00329441	86.4
	0.002	-0.00389462	102.1
Simplified Model 12: Cross Coupling Constraint	0.0005	-0.0030483	79.9
	0.00066	-0.00304902	79.9
	0.001	-0.00304624	79.9
	0.002	-0.00304202	79.8

Table B.5. Analysis time values of the models for configuration 2

Model Name	Mesh Size	Analysis Time (s)	Analysis Time Normalized
Full Model	0.0005	59183	315.9
	0.00066	18735	100.0
	0.001	2448	13.1
	0.002	247	1.3
Simplified Model 1: Full Model with Shell	0.0005	32879	175.5
	0.00066	37319	199.2
	0.001	10297	55.0
	0.002	2067	11.0
Simplified Model 2: Rigid Shank with Coupling	0.0005	5541	29.6
	0.00066	3099	16.5
	0.001	955	5.1
	0.002	185	1.0
Simplified Model 3: Coupling Constraint with Hole	0.0005	5178	27.6
	0.00066	2842	15.2
	0.001	663	3.5
	0.002	174	0.9

Table B.5. Analysis time values of the models for configuration 2 (continue)

Simplified Model 4: Coupling Constraint without Hole	0.0005	8998	48.0
	0.00066	3027	16.2
	0.001	977	5.2
	0.002	182	1.0
Simplified Model 5: Vertical Connector Beams	0.0005	-	-
	0.00066	2885	15.4
	0.001	760	4,1
	0.002	196	1.0
Simplified Model 6: Vertical Connector Beams On Washer Outer Line	0.0005	4670	24,9
	0.00066	2357	12.6
	0.001	612	3.3
	0.002	168	0.9
Simplified Model 7: Tie Constraint with Hole	0.0005	-	-
	0.00066	2679	14,3
	0.001	687	3.7
	0.002	125	0.7
Simplified Model 8: Tie constraint without hole	0.0005	9268	49.5
	0.00066	2961	15.8
	0.001	981	5.2
	0.002	176	0.9
Simplified Model 9: Connector One Beam	0.0005	3637	19.4
	0.00066	2046	10.9
	0.001	546	2.9
	0.002	184	1.0
Simplified Model 10: Cross Connector Beam	0.0005	8746	46.7
	0.00066	2719	14,5
	0.001	794	4,2
	0.002	186	1.0
Simplified Model 11: Rigid Shell Bolt	0.0005	5654	30.2
	0.00066	3322	17.7
	0.001	800	4,3
	0.002	191	1.0
Simplified Model 12: Cross Coupling Constraint	0.0005	3716	19.8
	0.00066	2720	14,5
	0.001	669	3.6
	0.002	171	0.9

Table B.5. Analysis time values of the models for configuration 2 (continue)

Simplified Model 13: Deformable Shell bolt	0.0005	7263	38.8
	0.00066	3804	20.3
	0.001	1202	6.4
	0.002	268	1.4

Table B.6. Maximum plastic strain values around the bolt hole on the frame of all models for configuration 2

Model Name	Mesh Size	Von Mises Stress Around The Hole on Plate (MPa)	Von mises Stress Normalized
Full Model	0.0005	460	100.4
	0.00066	458	100.0
	0.001	452	98.6
	0.002	431	94,2
Simplified Model 1: Full Model with Shell	0.0005	503	109.8
	0.00066	479	104,6
	0.001	459	100.2
	0.002	442	96.5
Simplified Model 2: Rigid Shank with Coupling	0.0005	443	96.7
	0.00066	428	93.4
	0.001	442	96.5
	0.002	419	91.5
Simplified Model 3: Coupling Constraint with Hole	0.0005	418	91.2
	0.00066	421	91.8
	0.001	419	91.5
	0.002	422	92.2
Simplified Model 4: Coupling Constraint without Hole	0.0005	435	95.0
	0.00066	435	95.0
	0.001	436	95.1
	0.002	416	90.8
Simplified Model 5: Vertical Connector Beams	0.0005		
	0.00066	1260	274,7
	0.001	534	116.5
	0.002	441	96.3
Simplified Model 6: Vertical Connector Beams On Washer Outer Line	0.0005	513	111.9
	0.00066	479	104,5
	0.001	457	99.6
	0.002	416	90.8

Table B.6. Maximum plastic strain values around the bolt hole on the frame of all models for configuration 2 (continue)

Simplified Model 7: Tie Constraint with Hole	0.0005	689	150.4
	0.00066	443	96.6
	0.001	1080	234,7
	0.002	435	95.0
Simplified Model 8: Tie constraint without hole	0.0005	449	98.0
	0.00066	444	97.0
	0.001	443	96.6
	0.002	429	93.7
Simplified Model 9: Connector One Beam	0.0005	1040	226.2
	0.00066	1350	295.7
	0.001	573	125.0
	0.002	518	113.0
Simplified Model10: Cross Connector Beam	0.0005	920	200.7
	0.00066	573	125.0
	0.001	550	120.0
	0.002	494	107.8
Simplified Model11: Rigid Shell Bolt	0.0005	458	99.9
	0.00066	478	104,3
	0.001	490	106.9
	0.002	472	102.9
Simplified Model 12: Cross Coupling Constraint	0.0005	447	97.5
	0.00066	442	96.6
	0.001	440	96.0
	0.002	436	95.2
Simplified Model 13: Deformable Shell Bolt	0.0005	527	115.0
	0.00066	539	117.6
	0.001	519	113.2
	0.002	482	105.1

Table B.7. Maximum plastic strain values around the bolt hole on the frame of all models for configuration 2

Model Name	Mesh Size	Max. Plastic Strain Around Hole on Plate	M P. Strain Normalized
Full Model	0.0005	0.113854	113.2
	0.00066	0.100572	100.0
	0.001	0.0963535	95.8
	0.002	0.0397501	39.5
Simplified Model 1: Full Model with Shell	0.0005	0.193439	192.3
	0.00066	0.167248	166.3
	0.001	0.126372	125.7
	0.002	0.109029	108.4
Simplified Model 2: Rigid Shank with Coupling	0.0005	0.0487256	48.4
	0.00066	0.0490493	48.8
	0.001	0.0497694	49.5
	0.002	0.0515128	51.2
Simplified Model 3: Coupling Constraint with Hole	0.0005	0.048012	47.7
	0.00066	0.047854	47.6
	0.001	0.0481288	47.9
	0.002	0.04798	47.7
Simplified Model 4: Coupling Constraint without Hole	0.0005	0.0618934	61.5
	0.00066	0.0510875	50.8
	0.001	0.0596607	59.3
	0.002	0.049658	49.4
Simplified Model 5: Vertical Connector Beams	0.0005	-	-
	0.00066	0.938396	933.1
	0.001	0.370281	368.2
	0.002	0.102859	102.3
Simplified Model 6: Vertical Connector Beams On Washer Outer Line	0.0005	0.246259	244,9
	0.00066	0.134148	133.4
	0.001	0.0957781	95.2
	0.002	0.0426296	42.4
Simplified Model 7: Tie Constraint with Hole	0.0005	0.112678	112.0
	0.00066	0.0571545	56.8
	0.001	0.065374	65.0
	0.002	0.0415348	41.3

Table B.7. Maximum plastic strain values around the bolt hole on the frame of all models for configuration 2 (continue)

Simplified Model 8: Tie constraint without hole	0.0005	0.0644172	64,1
	0.00066	0.063154	62.8
	0.001	0.0528945	52.6
	0.002	0.0424406	42.2
Simplified Model 9: Connector One Beam	0.0005	1.34374	1336.1
	0.00066	1.19464	1187.8
	0.001	0.68176	677.9
	0.002	0.305803	304,1
Simplified Model 10: Cross Connector Beam	0.0005	1.2808	1273.5
	0.00066	0.899226	894,1
	0.001	0.479061	476.3
	0.002	0.238121	236.8
Simplified Model 11: Rigid Shell Bolt	0.0005	0.101179	100.6
	0.00066	0.139909	139.1
	0.001	0.184715	183.7
	0.002	0.111873	111.2
Simplified Model 12: Cross Coupling Constraint	0.0005	0.0509267	50.6
	0.00066	0.0472789	47.0
	0.001	0.0446286	44,4
	0.002	0.0351254	34,9
Simplified Model 13: Deformable Shell Bolt	0.0005	0.293597	343.4
	0.00066	0.270417	316.3
	0.001	0.255851	299.3
	0.002	0.157737	184,5

Table B.8. Center displacement values all models for configuration 2

Model Name	Mesh Size	Central Displacement (m)	Center Displacement Normalized
Full Model	0.0005	-0.01514	101.0
	0.00066	-0.01499	100.0
	0.001	-0.01513	101.0
	0.002	-0.01342	89.5
Simplified Model 1: Full Model with Shell	0.0005	-0.01617	107.9
	0.00066	-0.01604	107.0
	0.001	-0.01595	106.4
	0.002	-0.01633	109.0
Simplified Model 2: Rigid Shank with Coupling	0.0005	-0.01299	86.7
	0.00066	-0.01299	86.7
	0.001	-0.01303	86.9
	0.002	-0.01306	87.2
Simplified Model 3: Coupling Constraint with Hole	0.0005	-0.01303	87.0
	0.00066	-0.01301	86.8
	0.001	-0.01301	86.8
	0.002	-0.01303	87.0
Simplified Model 4: Coupling Constraint without Hole	0.0005	-0.01289	86.0
	0.00066	-0.01292	86.2
	0.001	-0.01286	85.8
	0.002	-0.01287	85.9
Simplified Model 5: Vertical Connector Beams	0.0005	-	-
	0.00066	-0.01479	98.7
	0.001	-0.01403	93.6
	0.002	-0.01349	90.0
Simplified Model 6: Vertical Connector Beams On Washer Outer Line	0.0005	-0.01312	87.5
	0.00066	-0.01301	86.8
	0.001	-0.01296	86.4
	0.002	-0.01295	86.4
Simplified Model 7: Tie Constraint with Hole	0.0005	-0.01301	86.8
	0.00066	-0.01288	85.9
	0.001	-0.01224	81.6
	0.002	-0.01287	85.9
Simplified Model 8: Tie constraint without hole	0.0005	-0.01285	85.7
	0.00066	-0.01281	85.5
	0.001	-0.01283	85.6
	0.002	-0.01286	85.8

Table B.8. Center displacement values all models for configuration 2 (continue)

Simplified Model 9: Connector One Beam	0.0005	-0.02017	134,5
	0.00066	-0.01964	131.0
	0.001	-0.01866	124,5
	0.002	-0.01754	117.0
Simplified Model 10: Cross Connector Beam	0.0005	-0.01504	100.4
	0.00066	-0.01454	97.0
	0.001	-0.01424	95.0
	0.002	-0.01406	93.8
Simplified Model 11: Rigid Shell Bolt	0.0005	-0.0140131	91.3
	0.00066	-0.01475	98.4
	0.001	-0.01605	107.1
	0.002	-0.01659	110.7
Simplified Model 12: Cross Coupling Constraint	0.0005	-0.01281	85.4
	0.00066	-0.01279	85.3
	0.001	-0.01278	85.3
	0.002	-0.0128	85.4
Simplified Model 13: Deformable Shell Bolt	0.0005	0.01901	115.0
	0.00066	-0.01914	127.7
	0.001	-0.01927	128.6
	0.002	-0.01904	127.0

REFERENCES

1. E. S. Mistakidis and C. C. Baniotopoulos, "Steel T-Stub Connections Under Static Loading: an Effective 2-D Numerical Model", *L Construct. Steel Res.,* Vol. 44, Nos. 1-2, pp. 51-67, 1997.

2. O.S. Bursi and J.P. Jaspart, "Benchmarks for modeling of bolted connections", *J. Construct. Steel Res.* Vol. 43, Nos. 1-3, pp. 17-42, 1997.

3. O.S. Bursi and J.P. Jaspart, "Calibration of a Finite Element Model for Isolated Bolted End-Plate Steel Connections", *J. Construct. Steel Res.* Vol. 44, No. 3, pp. 225-262, 1997.

4. O.S. Bursi and J.P. Jaspart, "Basic issues in the finite element simulation of extended end plate connections", *Computers and Structures,* Vol. 69, pp. 361-382, 1998.

5. K.F. Chung and K.H. Ip, "Finite element modeling of bolted connections between cold formed steel strips and hot rolled steel plates under static shear loading", *Engineering Structures,* Vol. 22, pp. 1271–1284, 2000.

6. K.F. Chung and K.H. Ip, "Finite element investigation on the structural behaviour of coldformed steel bolted connections", *Engineering Structures,* Vol.23, pp. 1115–1125, 2001.

7. N. Kishi, A. Ahmed and N. Yabuki, "Nonlinear Finite Element Analysis of Top- And Seat-Angle with Double Web Angle Connections", *Structural Engineering and Mechanics*, Vol. 12, No. 2, pp. 201-214, 2001

8. J.A. Swanson, D.S. Kokan and R.T. Leon, "Advanced finite element modeling of bolted T-stub connection components", *Journal of Constructional Steel Research,* Vol. 58, pp. 1015–1031, 2002.

9. K.E. Barth, J.G. Orbison and R. Nukala, "Behavior of steel tension members subjected to uniaxial loading", *Journal of Constructional Steel Research,* Vol. 58, pp. 1103–1120, 2002.

10. A.M. Citipitioglu, R.M. Haj-Ali and D.W. White, "Refined 3D finite element modeling of partially-restrained connections including slip", *Journal of Constructional Steel Research,* Vol. 58, pp. 995–1013, 2002

11. S.-H. Ju, C.-Y. Fan and G.H. Wu, "Three-dimensional finite elements of steel bolted connections", *Engineering Structures,* Vol. 26, pp. 403–413, 2004.

12. C. Yorgun, S. Dalcı and G.A. Altay, "Finite element modeling of bolted steel connections designed by double channel", *Computers and Structures,* Vol. 82, pp. 2563–2571, 2004.

13. Jim Butterworth, "Finite Element Analysis of Structural Steelwork Beam to Column Bolted Connections", Constructional Research Unit, School of Science & Technology,University of Teesside, LUSAS Civil & Structural.

14. M.A. McCarthy , C.T. McCarthy, V.P. Lawlor and W.F. Stanley, "Three-dimensional finite element analysis of single-bolt, single-lap composite bolted joints: part I—model development and validation", *Composite Structures,* Vol. 71, pp. 140–158, 2005.

15. Young-Doo Kwon, H. Kwon, J. Hwangbo and S. Jang, "Finite element modeling for static and dynamic analysis of structures with bolted joint", *Key Engineering Materials*, Vols. 306-308, pp. 547-552, 2006.

16. Jeong Kim, Joo-Cheol Yoon, Beom-Soo Kang, "Finite Element Analysis and Modeling of Structure with Bolted Joints", *Applied Mathematical Modeling,* Vol. 31, pp. 895–911, 2007.

17. Tapan Sabuwala, Daniel Linzell and Theodor Krauthammer, "Finite element analysis of steel beam to column connections subjected to blast loads". *International Journal of Impact Engineering,* Vol. 31, pp. 861–876, 2005.

18. John D. Reid and Nicholas R. Hiser, "Detailed modeling of bolted joints with slippage", *Finite Elements in Analysis and Design,* Vol. 41, pp. 547–562, 2005.

19. Matthew Oldfield, Huajiang Ouyang, and John E. Mottershead, "Simplified models of bolted joints under harmonic loading", *Computers and Structures,* Vol. 84, pp. 25–33, 2005

20. Henrick And Wekezer Bart Hendricks and Jerry Wekezer, "Finite Element Modeling of G2 Guardrail". *Transportation Research Record,* Vol. 1528, pp. 130-137, 1996.

21. James L. O'Daniel, Kevin L. Koudela and Theodor Krauthammer, "Numerical Simulation and Validation of Distributed Impact Events", *International Journal of Impact Engineering*, Vol. 31, pp. 1013–1038, 2005.

22. http://en.wikipedia.org/wiki/ABAQUS

23. ABAQUS Analysis User's Manual, ABAQUS, Inc. 2004.

24. Hadi Razavia, Ali Abolmaalia and Mehdi Ghassemiehd, "Invisible elastic bolt model concept for finite element analysis of bolted connections", *Journal of Constructional Steel Research,* Vol. 63 pp. 647–657, 2007.

25. Wei Ren and Jianjun Wang, "Assembly-Induced Stress and Its Effect on the Integrity of Assembly System in Drop Simulation". *Proceedings of 7th International Conference on Thermal, Mechanical and Multiphysics Simulation and Experiments in Micro-Electronics and Micro-Systems, 24-26 April 2006,* pp. 1-7 EuroSime, 2006.